

1 **Inputs and processes affecting the distribution of particulate** 2 **iron in the North Atlantic along the GEOVIDE (GEOTRACES** 3 **GA01) section**

4
5
6 Arthur Gourain^{1,2}, H el ene Planquette¹, Marie Cheize^{1,3}, Nolwenn Lemaitre^{1,4}, Jan-Lukas
7 Menzel Barraqueta^{5, 6}, Rachel Shelley^{1, 7}, Pascale Lherminier⁸ and G eraldine Sarthou¹

8
9 1-UMR 6539/LEMAR/IUEM, CNRS, UBO, IRD, Ifremer, Technop ole Brest Iroise, Place Nicolas Copernic,
10 29280 Plouzan e, France

11 2- now at Ocean Sciences Department, School of Environmental Sciences, University of Liverpool, Liverpool,
12 L69 3GP, United Kingdom

13 3- now at Ifremer, Centre de Brest, G eosciences Marines, Laboratoire des Cycles G eochimiques (LCG), 29280
14 Plouzan e, France

15 4- now at Department of Earth Sciences, Institute of Geochemistry and Petrology, ETH-Z urich, Z urich,
16 Switzerland

17 5- GEOMAR, Helmholtz Centre for Ocean Research Kiel, Wischhofstra e 1-3, 24148 Kiel, Germany

18 6- now at Department of Earth Sciences, Stellenbosch University, Stellenbosch, 7600, South Africa

19 7- now at Earth, Ocean and Atmospheric Science, Florida State University, Tallahassee, Florida, 32310, USA

20 8- Ifremer, Univ. Brest, CNRS, IRD, Laboratoire d'Oc eanographie Physique et Spatiale (LOPS), IUEM, F-
21 29280, Plouzan e, France

22
23 *Correspondence to: helene.planquette@univ-brest.fr*

24 25 **Abstract**

26 The aim of the GEOVIDE cruise (May-June 2014, R/V *Pourquoi Pas?*) was to provide a better understanding of
27 trace metal biogeochemical cycles in the North Atlantic Ocean. As marine particles play a key role in the global
28 biogeochemical cycle of trace elements in the ocean, we discuss the distribution of particulate iron (PFe), in
29 relation to the distribution of particulate aluminium (PAI), manganese (PMn) and phosphorus (PP). Overall, 32
30 full vertical profiles were collected for trace metal analyses, representing more than 500 samples. This resolution
31 provides a solid basis for assessing concentration distributions, elemental ratios, size-fractionation, and adsorptive
32 scavenging processes in key areas of the thermohaline circulation. Total particulate iron concentrations ranged
33 from as low as 9 pmol L⁻¹ in surface waters of the Labrador Sea to 304 nmol L⁻¹ near the Iberian margin, while
34 median PFe concentrations of 1.15 nmol L⁻¹ were measured over the sub-euphotic ocean interior.

35 Within the Iberian Abyssal Plain, the ratio of PFe to PAI was identical to the continental crust molar ratio (0.21
36 mol mol⁻¹), indicating the important influence of crustal particles in the water column. Overall, the lithogenic
37 component explained more than 87% of PFe variance along the section. Within the Irminger and Labrador basins,

38 the formation of biogenic particles led to an increase of the PFe/PAI ratio (up to 0.64 mol mol⁻¹) compared to the
39 continental crust ratio. Continental margins provide high quantities of particulate trace elements (up to 10 nmol
40 L⁻¹ of PFe) to the open ocean. For example, horizontal advection of PFe was visible more than 250 km away from
41 the Iberian margin. Additionally, several benthic nepheloid layers were observed more than 200 m above the
42 seafloor along the transect, especially in the Icelandic, Irminger and Labrador basins, suspending particles with
43 high PFe content of up to 89 nmol L⁻¹.

44

45 **1. Introduction**

46 Particles play a key role in the ocean where they drive the residence time of most elements (Jeandel and Oelkers,
47 2015), and strongly influence the global biogeochemistry of macro- and micro-nutrients including iron (Milne et
48 al., 2017). In the surface ocean, biological activity produces biogenic suspended matter through planktonic
49 organisms, while atmospheric deposition (Baker et al., 2013; Jickells et al., 2005), riverine discharge (Aguilar-
50 Islas et al., 2013; Berger et al., 2008; Ussher et al., 2004) or ice-melting (Hawkings et al., 2014; Lannuzel et al.,
51 2011, 2014) deliver mostly lithogenic derived particles to surface waters. These particulate inputs are highly
52 variable, both spatially and seasonally, in the world's oceans. At depth, benthic and shelf sediment resuspension
53 (e.g. Aguilar-Islas et al., 2013; Cullen et al., 2009; Elrod et al., 2004; Fitzwater et al., 2000; Hwang et al., 2010;
54 Lam et al., 2015; Lam and Bishop, 2008; McCave and Hall, 2002), and hydrothermal activity (Elderfield and
55 Schultz, 1996; Lam et al., 2012; Tagliabue et al., 2010, 2017; Trefry et al., 1985), provides important amounts of
56 particles to the water column. Moreover, authigenic particles can be produced *in-situ* by aggregation of colloids
57 (Bergquist et al., 2007) or oxidation processes (Bishop and Fleisher, 1987; Collier and Edmond, 1984). Thus,
58 oceanic particles result from a complex combination of these different sources and processes (Lam et al., 2015).
59 In the upper water column, the total iron pool is dominated by marine particles (Radic et al., 2011) which strongly
60 interact with the dissolved pool (e.g. Ellwood et al., 2014). Indeed, dissolved iron can be scavenged onto particles
61 (Gerringa et al., 2015; Rijkenberg et al., 2014), incorporated into biogenic particles (Berger et al., 2008) or
62 produced by remineralisation of particles (Dehairs et al., 2008; Sarthou et al., 2008). Interestingly, the concept of
63 “reversible scavenging” (i.e. release at depth of dissolved iron previously scavenged onto particles) has been
64 advocated recently (Dutay et al., 2015; Jeandel and Oelkers, 2015; Labatut et al., 2014), while other studies reveal
65 distinct dissolution processes of inorganic particulate iron (e.g. Oelkers et al., 2012; Cheize et al., 2018). Slow
66 dissolution of particulate iron at margins has also been evoked as a continuous fertilizer of primary production
67 and should be considered as a source of dissolved iron (e.g. Jeandel et al., 2011; Jeandel and Oelkers, 2015; Lam
68 and Bishop, 2008). Within or below the mixed layer, the rates of regeneration processes can also impact the
69 bioavailable pool of iron, among other trace metals (e.g. Ellwood et al., 2014; Nuester et al., 2014). However, the
70 rates of these processes are not yet fully constrained. The study of particulate iron is thus essential to better
71 constrain its marine biogeochemical cycle. Interest has grown in this subject over the last 10 years, in particular
72 (e.g. Bishop and Biscaye, 1982; Collier and Edmond, 1984; Frew et al., 2006; Lam et al., 2012; Milne et al., 2017;
73 Planquette et al., 2011, 2013; Sherrell et al., 1998) and, to our knowledge, only two studies have been performed
74 on an ocean-wide scale: the GA03 GEOTRACES North Atlantic Zonal Transect (Lam et al., 2015; Ohnemus and
75 Lam, 2015) and the GP16 GEOTRACES Pacific Transect (Lam et al., 2017; Lee et al., 2017).

76 Within this global context, this paper presents the particulate iron distribution of the North Atlantic Ocean, along
77 the GEOTRACES GA01 section (GEOVIDE), and discusses the various sources and processes affecting

78 particulate iron (PFe) distribution, using particulate aluminium (PAI), phosphorus (PP) or manganese (PMn)
79 distributions to support our conclusions.

80

81 **2. Methods**

82 *2.1. Study area*

83 Particulate samples were collected at 32 stations during the GEOVIDE (GEOTRACES GA01 section) cruise
84 between May and June 2014 aboard the R/V *Pourquoi Pas?* in the North Atlantic Ocean (Sarhou et al., 2018).
85 The sampling spanned several biogeochemical provinces (Figure 1), starting over the Iberian margin (IM, Stations
86 2, 4 and 1), and proceeding to the Iberian Abyssal Plain (IAP, Stations 11 to 17), the Western European Basin
87 (WEB, Station 19 to Station 29) and the Icelandic Basin (IcB, Stations 32 to 36). Then, samples were collected
88 above the Reykjanes Ridge (RR, Station 38), in the Irminger Basin (IrB, Stations 40 to 60), close to the Greenland
89 shelf (GS, Stations 53, 56 and 61), the Labrador Basin (LB, Stations 63 to 77) and finally close the Newfoundland
90 shelf (NS, Station 78) (Figure 1). The North Atlantic is characterized by a complex circulation (briefly described
91 in section 3.1 and in detail by Zunino et al. (2017) and García-Ibáñez et al. (2015)) and is one of the most
92 productive regions of the global ocean (Martin et al., 1993; Sanders et al., 2014).

93

94

95 *2.2. Sampling*

96 Samples were collected using the French GEOTRACES clean rosette, equipped with twenty-two 12 L GO-FLO
97 bottles (two bottles were leaking and were not deployed during the cruise). GO-FLO bottles (General Oceanic's)
98 were initially cleaned in the home laboratory (LEMAR) following the GEOTRACES procedures (Cutter and
99 Bruland, 2012). The rosette was deployed on a 14 mm Kevlar cable with a dedicated, custom-designed clean
100 winch. Immediately after recovery, the GO-FLO bottles were individually covered at each end with plastic bags
101 to minimize contamination. Bottles were then transferred into a clean container (class-100) for sampling. On each
102 cast, nutrient and/or salinity samples were taken to check potential leakage of the GO-FLO bottles.

103 Filters were cleaned following the GEOTRACES protocols (<http://www.geotraces.org/images/Cookbook.pdf>)
104 and kept in acid-cleaned 1 L LDPE bottles (Nalgene) filled with ultrapure water (Milli-Q, resistivity of 18.2 M Ω
105 cm) until use. All filters were 25 mm diameter in order to optimize the signal over the filter blank, except at the
106 surface depth where 47 mm diameter filters were used. The filters were mounted on acid-cleaned polysulfone
107 filter holders (NalgeneTM). Prior to filtration, the GO-FLO bottles were shaken three times, as recommended in
108 the GEOTRACES cookbook to avoid settling of particles in the lower part of the bottle. GO-FLO bottles were
109 pressurized to < 8 psi with 0.2 μ m filtered nitrogen gas (N₂, Air Liquide). Seawater was then filtered directly
110 through paired filters (Pall Gelman SuporTM 0.45 μ m polyetersulfone, and Millipore mixed ester cellulose MF 5
111 μ m) mounted in Swinnex polypropylene filter holders (Millipore), following Planquette and Sherrell (2012) inside
112 the clean container. Filtration was operated until the bottle was empty or until the filter clogged; the volume
113 filtered ranged from 2 L for surface samples to 11 L within the water column. After filtration, filter holders were
114 disconnected from the GO-FLO bottles and a gentle vacuum was applied using a syringe in order to remove any
115 residual water under a laminar flow hood. Filters were then removed from the filter holders with plastic tweezers
116 (which were rinsed with Milli-Q between samples). Most of the remaining seawater was removed via 'sipping'

117 by capillary action, when placing the non-sampled side of the filter onto a clean 47 mm supor filter. Each filter
118 pair was then placed in an acid-cleaned polystyrene PetriSlide (Millipore), double bagged, and finally stored at -
119 20 °C until analysis at LEMAR. Between casts, filter holders were thoroughly rinsed with Milli-Q, placed in an
120 acid bath (5% Trace metal grade HCl) for 24 hours, then rinsed with Milli-Q.

121 At each station, process blanks were collected as follows: 2 L of a deep (1000 m) and a shallow (40 m) seawater
122 sample were first filtered through a 0.2 µm pore size capsule filter (Pall Gelman Acropak 200) mounted on to the
123 outlet of the GO-FLO bottle before passing through the particle sampling filter, which was attached directly to
124 the swinnex filter holder.

125

126 2.3. Analytical methods

127 In the home laboratory, sample handling was performed inside a clean room (Class 100). All solutions were
128 prepared using ultrapure water (Milli-Q) and all plasticware had been acid-cleaned before use. Frozen filters,
129 collected within the mixed layer or within nepheloid layers, were first cut in half using a ceramic blade: one filter
130 half was dedicated to total digestion (see below), while the other half was archived at -20 °C for SEM analyses or
131 acid leaching of “labile” metals (Berger et al., 2008; to be published separately).

132 Filters were digested following the method described in Planquette and Sherrell (2012). Filters were placed on
133 the inner wall of acid-clean 15 mL PFA vials (Savillex™), and 2 mL of a solution containing 2.9 mol L⁻¹
134 hydrofluoric acid (HF, suprapur grade, Merck) and 8 mol L⁻¹ nitric acid (HNO₃, Ultrapur grade, Merck) was added
135 to each vial. Vials were then closed and refluxed at 130 °C on a hot plate for 4 hours, after which the filters were
136 removed. After cooling, the digest solution was evaporated at 110 °C to near dryness. Then, 400 µL of
137 concentrated HNO₃ (Ultrapur grade, Merck) was added, and the solution was re-evaporated at 110 °C. Finally,
138 the obtained residue was dissolved with 3 mL of 0.8 mol L⁻¹ HNO₃ (Ultrapure grade, Merck). This archived
139 solution was transferred to an acid cleaned 15 mL polypropylene centrifuge tube (Corning®) and stored at 4 °C
140 until analyses.

141 All analyses were performed on a sector field inductively coupled plasma mass spectrometer (SF-ICP-MS
142 Element 2, Thermo-Fisher Scientific). Samples were diluted by a factor of 7 on the day of analysis in acid-washed
143 13 mm (outer diameter) rounded bottom, polypropylene centrifuge tubes (VWR) with 0.8 mol L⁻¹ HNO₃ (Ultrapur
144 grade, Merck) spiked with 1 µg L⁻¹ of indium (¹¹⁵In) solution in order to monitor the instrument drift. Samples
145 were introduced with a PFA-ST nebulizer connected to a quartz cyclonic spray chamber (Elemental Scientific
146 Incorporated, Omaha, NE) via a modified SC-Fast introduction system consisting of an SC-2 autosampler, a six-
147 port valve and a vacuum-rinsing pump. The autosampler was contained under a HEPA filtered unit (Elemental
148 Scientific). Two 6-point, matrix-matched multi-element standard curves with concentrations bracketing the range
149 of the samples were run at the beginning, the middle and the end of each analytical run. Analytical replicates were
150 made every 10 samples, while accuracy was determined by performing digestions of the certified reference
151 material BCR-414 (plankton, Community Bureau of Reference, Commission of the European Communities),
152 PACS-3 and MESS-4 (marine sediments, National Research Council Canada), following the same protocol used
153 for the samples. Recoveries were typically within 10% of the certified values (and within the error of the data,
154 taken from replicate measurements, Table 1). Once all data were normalized to an ¹¹⁵In internal standard and
155 quantified using an external standard curve, the dilution factor of the total digestion was accounted for. The

156 elemental concentrations were obtained per filter (pmol/filter) and were then process blank-corrected. Finally,
157 pmol/filter values were divided by the volume of water filtered through stacked filters.
158 Total concentrations (sum of small size fraction (0.45-5 µm) and large (>5 µm) size fraction) of particulate trace
159 elements are reported in Table S1.

160

161 2.4. Positive matrix factorisation

162 Positive Matrix Factorisation (PMF) was run to characterise the main factors influencing the particulate trace
163 element variance along the GEOVIDE section. In addition to PFe, PAI, PMn, and PP, nine additional elements
164 were included in the PMF: yttrium (Y), barium (Ba), lead (Pb), thorium (Th), titanium (Ti), vanadium (V), cobalt
165 (Co), copper (Cu) and zinc (Zn). The PMF was conducted on samples where all elements were above their
166 detection limits; after selection, 445 of the 549 existing data points were used. Analyses were performed using
167 the PMF software, EPA PMF 5.0, developed by the USA Environmental Protection Agency (EPA). Three to six
168 factor models were run on the data. The configuration that provided the lowest error estimation (i.e. was the most
169 reliable) was the four factor model. To ensure stability, this model was run 100 times. After displacement, error
170 estimation and bootstrap error estimation, the model was recognised as stable.

171

172 2.5. Derived and ancillary parameters

173 To investigate the proportion of lithogenic iron within the bulk particulate iron, we used the Upper Continental
174 Crust (UCC) Fe/Al molar ratio (0.21) of Taylor and McLennan (1995) to calculate the lithogenic components of
175 particles (%PFe_{litho}) following Eq. (1):

176

$$177 \quad \%PFe_{litho} = 100 * \left(\frac{PAI}{PFe} \right)_{sample} * \left(\frac{PFe}{PAI} \right)_{UCCratio} \quad (1)$$

178

179 The non-lithogenic PFe is obtained using Eq. (2):

180

$$181 \quad \%PFe_{non_litho} = 100 - \%PFe_{litho} \quad (2)$$

182

183 Note that while the %PFe_{litho} and %PFe_{non-litho} proxies are interesting tools to evaluate the importance of lithogenic
184 and non-lithogenic (either biogenic or authigenic) fraction, they have to be used carefully, as the spatial and
185 temporal variation of the lithogenic component ratios may involve uncertainties of the estimated fraction value.

186 In addition to PAI, PMn can be used as a tracer of inputs from shelf resuspension (Lam and Bishop, 2008), using
187 a percentage of sedimentary inputs “%bulk sediment inputs” estimated according to the following equation:

$$188 \quad \%bulksedimentPMn = 100 * \left(\frac{PAI}{PMn} \right)_{sample} * \left(\frac{PMn}{PAI} \right)_{UCCratio} \quad (3)$$

189 with PAI/PMn being the ratio from the GEOVIDE samples and the PMn/PAI being the UCC value (0.0034; Taylor
190 and McLennan, 1995).

191 This proxy can be a good indicator of sediment resuspension. We assume that particles newly resuspended in the
192 water column will have the same PMn/PAI ratio as the UCC ratio, leading to a “%bulk sediment Mn” of 100%.
193 This proxy assumes homogeneity of the sediment PMn/PAI ratio throughout the GEOVIDE section. However,
194 this may not be the case at every station. In consequence, this proxy should only be used to identify new benthic
195 resuspension at specific locations; inter-comparison between several locations may not be appropriate. When a
196 sample presents a “%bulk sediment Mn” greater than 100%, we have assigned a maximum value of 100%. As the
197 Mn cycle can also be influenced by biotic uptake (e.g. Peers and Price, 2004; Sunda and Huntsman, 1983), this
198 proxy is only used at depths where biologic activity was negligible (i.e. below 150m depth).

199 Potential temperature (θ°), salinity (S), and transmissometry data were retrieved from the CTD sensors (CTD
200 SBE911 equipped with a SBE43).

201

202

203 **3. Results**

204 *3.1. Hydrography setting*

205 Here, we briefly describe the hydrography encountered during the GEOVIDE section (Figure 2) as a thorough
206 description is available in García-Ibáñez et al. (2015). At the start of the section, the warm and salty Mediterranean
207 Water (MW, $S = 36.50$, $\theta^\circ = 11.7$ °C) was sampled between 600 and 1700 m in the Iberian Abyssal Plain (IAP).
208 MW resulted from the mixing between the Mediterranean Overflow Water (MOW) plume coming from the
209 Mediterranean Sea and local waters. Surface water above the Iberian Shelf was characterised by low salinity ($S =$
210 34.95) at station 2 and 4 compared to surrounding water masses. Close to the floor of the Iberian Abyssal Basin,
211 the North East Atlantic Deep Water (NEADW, $S = 34.89$, $\theta^\circ = 2.0$ °C) spread northward. The North Atlantic
212 Central Water (NACW, $S > 35.60$, $\theta^\circ > 12.3$ °C) was the warmest water mass of the transect and was observed in
213 the subsurface layer of the Western European Basin and Iberian Abyssal Plain. An old Labrador Sea Water (LSW,
214 $S = 34.87$, $\theta^\circ = 3.0$ °C) flowed inside the Western European and Icelandic Basins, between 1000 and 2500m
215 depth.

216 In the Icelandic Basin, below the old LSW, the Iceland-Scotland Overflow Water (ISOW, $S = 34.98$, $\theta^\circ = 2.6$ °C)
217 spread along the Reykjanes Ridge slope. This cold water, originating from the Arctic, led to the formation of
218 NEADW after mixing with surrounding waters. North Atlantic hydrography was impacted by the northward
219 flowing of the North Atlantic Current (NAC), which carried warm and salty waters from the subtropical area. Due
220 to air-sea interactions and mixing with surrounding water, the NACW is cooled and freshened in the subpolar
221 gyre and is transformed in Subpolar Mode Water (SPMW). The formation of SPMW inside the Icelandic and
222 Irminger Basins leads to the formation of regional mode waters: the Iceland Subpolar Mode Water (IcSPMW, S
223 $= 35.2$, $\theta^\circ = 8.0$ °C) and the Irminger Subpolar Mode Water (IrSPMW, $S = 35.01$, $\theta^\circ = 5.0$ °C), respectively.
224 IcSPMW was a relatively warm water mass with potential temperature up to 7 °C (García-Ibáñez et al., 2015).
225 Another branch of the NAC mixed with Labrador Current waters to form the relatively fresh SubArctic
226 Intermediate Water (SAIW, $S = < 34.8$, 4.5 °C $< \theta^\circ < 6$ °C).

227 The Irminger Basin is a complex area with a multitude of water masses. In the middle of the basin, an old LSW,
228 formed one year before (Straneo et al., 2003), spread between 500 and 1200 m depth. Close to the bottom, the

229 Denmark Strait Overflow Water (DSOW, $S = 34.91$) flowed across the basin. Greenland coastal waters were
230 characterised by low salinity values, down to $S = 33$. The strong East Greenland Current (EGC) flowed southward
231 along the Greenland shelf in the Irminger Basin. At the southern tip of Greenland, this current enters the Labrador
232 Basin along the west coast of Greenland and followed the outline of the basin until the Newfoundland shelf. In
233 the Labrador Basin, the deep convection of SPMW at 2000 m was involved in the formation of the LSW ($S =$
234 34.9 , $\theta = 3.0^{\circ}\text{C}$) (García-Ibáñez et al., 2015; Yashayaev and Loder, 2009). Above the Newfoundland Shelf,
235 surface waters were affected by discharge from rivers and ice-melting and characterised by extremely low salinity
236 for open ocean waters, below 32 in the first 15 meters.

237 3.2. Section overview

238 Total particulate concentrations spanned a large range of concentrations from below detection (Table 1) to 304
239 nmol L^{-1} for PFe, 1544 nmol L^{-1} for PAI, 3.5 nmol L^{-1} for PMn and 402 nmol L^{-1} for PP. The ranges of
240 concentrations are comparable to other studies recently published (Table 2).

241 Along the section, PFe, PAI, and PMn were predominantly found ($> 90\%$) in particles larger than $5 \mu\text{m}$, except
242 in surface waters, reflecting a more heterogenous pattern, where $9 \pm 8.6\%$ of PFe, $10.9 \pm 15.4\%$ of PAI and 32.8
243 $\pm 16.6\%$ of PMn, $38.8 \pm 8.6\%$ of PP were hosted by smaller particles ($0.45\text{-}5 \mu\text{m}$). Data are shown in Figure 3.

244

245 3.3. Open Ocean stations: from the Iberian Abyssal Plain to the Labrador Basin

246 This concerns all stations from station 11 to 77, with the exception of stations 53, 56 and 61 which were sampled
247 close to the Greenland coast (Figure 1). Particulate iron concentration profiles showed identical patterns at all the
248 open ocean stations encountered along the section. Median PFe was low at 0.25 nmol L^{-1} within the first 100 m
249 and steadily increased with depth. However, at two stations, elevated concentrations were determined in the upper
250 100 m, up to 4.4 nmol L^{-1} at station 77 at 40 m depth and 7 nmol L^{-1} at station 63 between 70 and 100 m depth.
251 PFe concentrations gradually increased with depth, with a median PFe of 1.74 nmol L^{-1} below 1000m. Close to
252 the seafloor of some stations (26, 29, 32, 34, 49, 60, and 71), high concentrations of PFe were observed, up to 88
253 nmol L^{-1} (station 71 at 3736 m). These high PFe values were associated with low beam transmissometry values \leq
254 97% .

255 Particulate aluminium and manganese profiles were similar to PFe profiles, with low concentrations measured in
256 the first 100 m (1.88 nmol L^{-1} and 55 pmol L^{-1} , respectively) which increased towards the seafloor. Close to the
257 seafloor, high concentrations were determined at the same stations cited above for PFe, with a maximum of 264
258 nmol L^{-1} and 3.5 nmol L^{-1} for PAI and PMn respectively at station 71 (supplementary Table S1). Highest
259 particulate phosphorus concentrations were in the uppermost 50 m, with a median value of 66 nmol L^{-1} . Below
260 200 m depth PP concentrations decreased to values below 10 nmol L^{-1} . Inter-basins differences were observed
261 within surface samples, with median PP concentration being higher in the Irminger Basin (127 nmol L^{-1}) than in
262 the Iberian Abyssal Plain (28 nmol L^{-1}) (Figure 3).

263 Finally, above the Reykjanes Ridge, PP, PMn, PAI and PFe concentrations were in the same range as the
264 surrounding open ocean stations. However, close to the seafloor, high concentrations were measured, with PFe,

265 PAI, and PMn reaching 16.2 nmol L⁻¹, 28.8 nmol L⁻¹, and 0.51 nmol L⁻¹ at 1354 m depth, respectively (Figure 3
266 and Table S1).

267

268 3.4. Margins and Shelves: Iberian Margin (stations 1 to 4), Greenland coast (stations 53, 56
269 and 61) and Newfoundland Shelf (station 78)

270

271 The Iberian margin was characterised by low beam transmissometry values at station 2 (88 % at 140 m depth,
272 Figure 4a) suggesting high particle concentrations. Particulate iron concentrations varied from 0.02 nmol L⁻¹ to
273 304 nmol L⁻¹. Within the first 50 m, PFe concentrations decreased towards the shelf break where PFe dropped
274 from 2.53 nmol L⁻¹ (station 2) to 0.8 nmol L⁻¹ (Station 1). At all three stations, PFe concentrations increased with
275 depth and reached a maximum close to the seafloor. For example, 300 nmol L⁻¹ of PFe was determined at 138.5
276 m depth at station 2. Lithogenic tracers, such as PAI or PMn, presented similar profiles to PFe with concentrations
277 ranging from 0.11 and 1544 nmol L⁻¹, and from below detection limit to 2.51 nmol L⁻¹, respectively (Figure 3,
278 Table S1). Total particulate phosphorus concentrations were relatively low in surface waters ranging from values
279 below detection to 38 nmol L⁻¹; concentrations decreased with depth and were less than 0.7 nmol L⁻¹ below 1000
280 m depth.

281 In the vicinity of the Greenland shelf, PFe concentrations had a high median value of 10.8 nmol L⁻¹ and were
282 associated with high median PAI and PMn concentrations of 32.3 nmol L⁻¹ and 0.44 nmol L⁻¹, respectively.
283 Concentrations of PP were high at the surface with a value of 197 nmol L⁻¹ at 25 m depth of station 61. Then, PP
284 concentrations decreased strongly, to less than 30 nmol L⁻¹ below 100 meters depth. Furthermore, beam
285 transmissometry values in surface waters at these three stations, were the lowest of the entire section, with values
286 below 85 % (Figure 4a).

287 Close to the Newfoundland margin, surface waters displayed a small load of particulate trace metals as PFe, PAI,
288 and PMn concentrations were below 0.8 nmol L⁻¹, 2 nmol L⁻¹, and 0.15 nmol L⁻¹, respectively. Then, close to the
289 bottom of station 78, at 371 m depth, beam transmissometry values dropped to 94 % (Figure 4a) and were
290 associated with extremely high concentrations of PFe = 168 nmol L⁻¹, PAI = 559 nmol L⁻¹, and PMn = 2 nmol L⁻¹.
291 Total PP concentrations in the first 50 m ranged from 35 to 97 nmol L⁻¹. Below 50 m, PP remained relatively
292 high with values up to 16 nmol L⁻¹ throughout the water column. (Figure 3 and Table S1).

293

294 **4. Discussion**

295 Our goal was to investigate mechanisms that drive the distribution of PFe in the North Atlantic, in particular the
296 different routes of supply and removal. Possible sources of PFe include lateral advection offshore from margins,
297 atmospheric inputs, continental run-off, melting glaciers and icebergs, resuspended sediments, hydrothermal
298 inputs and biological uptake. Removal processes include remineralization, dissolution processes and sediment
299 burial.

300 In the following sections, we examine each of these sources and processes, explore the evidence for their relative
301 importance, and use compositional data to estimate the particle types and host phases for iron and associated
302 elements.

303 4.1. Analysis of the principal factors controlling variance: near-ubiquitous influence of crustal
304 particles in the water column

305 Positive matrix factorisation analysis (Figure 5) was undertaken on the entire dataset, in consequence, the factors
306 described below are highly influenced by the major variations of particulate element concentrations (usually at
307 the interfaces, i.e. margin, seafloor, surface layer). The first factor is characterised by lithogenic elements,
308 representing 86.8 % of the variance of PFe, 75.8 % of PAI and 90.5 % of PTi. The second factor is correlated with
309 both Mn and Pb and explains no less than 76.5 % and 77.0 % of their respective variances. Ohnemus and Lam
310 (2015) observed this co-relation between manganese and lead particles and explained it by the co-transport on
311 Mn-oxides (Boyle et al., 2005). The formation of barite explains the third factor and constrained 87.7 % of the Ba
312 variance in the studied regions. Biogenic barite accumulation within the mesopelagic layer is related to bacterial
313 activity and remineralisation of biogenic material (Lemaitre et al., 2018a). A biogenic component is the fourth
314 factor and explained most of PP variance, 83.7 %. The micronutrient trace metals, copper, cobalt and zinc, had
315 more than a quarter of their variances influenced by this factor. Note that the biogenic contribution to PFe and
316 other trace elements will be discussed in another paper (Planquette et al., in prep).

317 These results indicate that along the GA01 section, PFe distributions were predominantly controlled by lithogenic
318 material and to a smaller extent by remineralisation processes (as seen by a factor 3 contribution of 4.1 %). This
319 does not rule out some biogenic influences on PFe distribution, especially in the surface, but this contribution is
320 obscured by the high lithogenic contribution.

321 To further investigate the influence of crustal material on the distribution of PFe, it is instructive to examine the
322 distribution of the PFe to PAI molar ratio, and the resulting %PFe_{litho} (see section 2.6 for definition of this
323 parameter) along the section (Figure 6). Overall, the estimated lithogenic contribution to PFe varies from 25 %
324 (west of the Irminger Basin, station 60, 950 m depth) to 100 % at stations located within the Western European
325 Basin. Note that 100% of estimated lithogenic PFe does not necessary mean that biogenic particles are absent;
326 they may just be masked by the dominance of lithogenic particles. Important inter-basin variations are observed
327 along the section (Figure 6). The IAP and WEB are linked with high median values of the proxy %PFe_{litho}, 90 %
328 (Figure 6b), which is also reflected in the MW and NEADW PFe/PAI ratio which displays a value close to the
329 crustal one (Figure 7). This could be linked to the lateral advection of iron rich lithogenic particles sourced from
330 the Iberian margin and to atmospheric inputs (Shelley et al., 2017). The atmospheric external source is discussed
331 in more detail in section 4.2.4. Then, between stations 26 and 29, the %PFe_{litho} proxy values dramatically
332 decreased, and reached values less than 55 % in the Iceland, Irminger and the Labrador basins (Figure 6b). This
333 feature is likely associated with the presence of the Sub-Arctic Front, located between 49.5 and 51 °N latitude and
334 23.5 and 22 °W longitude (Zunino et al., 2017). Indeed, this front which separates cold and fresh water of subpolar
335 origin from warm and salty water of subtropical origin was clearly identifiable by the steep gradient of the
336 isohalines between station 26 and 29; salinity dropping from 35.34 to 35.01 (Figure 2). North of the Sub-Arctic
337 Front, LSW and ISOW display high PFe/PAI ratios, ranging from 0.36 to 0.44 mol mol⁻¹ (Figure 6a). These high
338 ratios, compared to the crustal one (i.e. 0.21), could be associated with higher proportions of PFe from biogenic
339 origin, especially in the case of the LSW.

340

341 4.2. Tracking the different inputs of particulate iron

342

4.2.1. Inputs at margins: Iberian, Greenland and Newfoundland

343 Inputs of iron from continental margin sediments supporting the high productivity found in shallow coastal regions
344 have been demonstrated in the past (e.g. Cullen et al. 2009, Elrod et al. 2004, Jeandel et al. 2011, Ussher et al.
345 2007) and sometimes, were shown to be advected at great distances from the coast (e.g. Lam and Bishop, 2008).
346 In the following section, we will investigate these possible sources in proximity to the different margins
347 encountered.

348

349 *The Iberian margin*

350 The Iberian margin was an important source of lithogenic-derived iron-rich particles to the Atlantic Ocean during
351 GEOVIDE; shelf resuspension impacts were perceptible up to 280 km from the margin (Station 11) in the Iberian
352 Abyssal Plain (Figure 8).

353 On the shelf, at station 2, high sediment resuspension resulted in the low beam transmissometry value (87.6 %) at
354 the immediate vicinity of the seafloor (153 m depth). This sediment resuspension led to an extensive input of
355 lithogenic particles within the water column associated with high concentrations of PFe (304 nmol L⁻¹), PAI (1500
356 nmol L⁻¹), and PMn (2.5 nmol L⁻¹) (Figure 3, Table S1). Moreover, 100 % of PFe was estimated to have a
357 lithogenic origin (Figure 8b) while 100 % of the PMn was estimated to be the result of a recent sediment
358 resuspension according to the %PFe_{litho} and “%bulk sediment Mn” proxies (Figure 8b and c), confirming the
359 resuspended particle input. In addition, ADCP data acquired during GEOVIDE (Zunino et al., 2017) and several
360 other studies have reported an intense current spreading northward coming from the Straits of Gibraltar and
361 Mediterranean Sea, leading to the strong resuspension of benthic sediments above the Iberian Shelf (e.g. Biscaye
362 and Eittrheim, 1977, Eittrheim et al., 1976, McCave and Hall, 2002, Spinrad et al., 1983).

363 At distance from the shelf, within the Iberian Abyssal Plain, an important lateral advection of PFe from the margin
364 was observable (Figure 8a). These lateral inputs occurred at two depth ranges: between 400 and 1000 m as seen
365 at stations 4 and 1, with PFe concentrations reaching 4 nmol L⁻¹, and between 2500 m and the bottom (3575 m)
366 of station 1, with PFe concentrations reaching 3.5 nmol L⁻¹. While 100 % of PFe had a lithogenic signature, the
367 sedimentary source input estimation decreased, between 40 % and 90 % of the PMn (Figure 8b). Transport of
368 lithogenic particles was observable until station 11 (12.2°W) at 2500 m where PFe concentration was 7.74 nmol
369 L⁻¹ and 60 % of PMn had a sedimentary origin (Figure 4). It is noteworthy that no increase in PFe, PMn or PAI
370 was observed between 500 and 2000 m depth, where the MOW spreads (García-Ibáñez et al., 2015). This is
371 consistent with the observed dissolved iron (DFe) concentrations (Tonnard et al., 2018, this issue), yet in contrast
372 to dissolved aluminium (DAI) concentrations (Menzel-Barraqueta et al., 2018, this issue) which were high in the
373 MOW, and with the study of Ohnemus and Lam (2015) that reported a maximum PFe concentration at 695 m
374 depth associated with the particle-rich Mediterranean Overflow Water (Eittrheim et al., 1976) in the IAP. However,
375 their station was located further south of our station 1. The shallower inputs observed at stations 1 and 4 could
376 therefore be attributed to sediment resuspension from the Iberian margin and nepheloid layer at depth for station
377 1.

378 Surface coastal waters of the Iberian Shelf are impacted by the runoff for the Tagus River, which is characterised
379 by high suspended matter discharges, ranging between 0.4 to 1 × 10⁶ tons yr⁻¹, and with a high anthropogenic
380 trace element signature (Jouanneau et al., 1998). During the GEOVIDE section, the freshwater input was

381 observable at stations 1, 2 and 4 in the first 20 m; salinity was below 35.2 while surrounding water masses had
382 salinity up to 35.7. Within the freshwater plume, particulate concentrations were high at station 2 with PFe of 1.83
383 nmol L^{-1} . Further away from the coast, the particulate concentrations remained low at 20m depth, with PFe, PAI,
384 and PMn concentrations of 0.77 nmol L^{-1} , 3.5 nmol L^{-1} , and 0.04 nmol L^{-1} , respectively at station 1. The low
385 expansion of the Tagus plume is likely due to the rapid settling of suspended matter. Indeed, our coastal station 2
386 was located approximately 50 km from the Iberian coast, whereas the surface particle load can only be observed
387 at a maximum distance of 30 km from the Tagus estuary (Jouanneau et al., 1998). Overall, the Iberian margin
388 appears to be an important source of lithogenic-derived iron rich particles in the Atlantic Ocean.

389

390 *South Greenland*

391 During GEOVIDE, the Greenland shelves were a source of particulate-rich meteoric water leading to a transfer
392 of DFe to PFe by enhanced biological activity. Indeed, both East (station 53) and West (station 61) Greenland
393 shelves had high concentration of particles (beam transmissometry of 83 %, Figure 4a) and particulate trace
394 elements, reaching 22.1 nmol L^{-1} (at 100 m depth) and 18.7 nmol L^{-1} (at 136 m depth) of PFe, respectively. Several
395 studies have already demonstrated the importance of icebergs and sea ice melting as sources of dissolved and
396 particulate iron (e.g. van der Merwe et al., 2011a, 2011b; Planquette et al., 2011; Raiswell et al., 2008). The
397 Greenland shelf is highly influenced by external fresh water inputs such as sea-ice-melting or riverine runoff
398 (Fragoso et al., 2016), which are important sources of iron to the Greenland Shelf (Bhatia et al., 2013; Hawkings
399 et al., 2014; Statham et al., 2008). During the cruise, the relative freshwater observed ($S < 33$ psu) within the first
400 25 m of stations 53 and 61 was associated with high PFe (19 nmol L^{-1}), PAI (61 nmol L^{-1}), PMn (0.6 nmol L^{-1})
401 and low beam transmissometry ($\leq 85\%$) (Figure 4a and Table S1). The associated particles were enriched in iron
402 compared to aluminium, as PFe/PAI ratio was 0.3 within the meteoric water plume. The high PP concentrations
403 (reaching 197 nmol L^{-1}) resulting from high biological production, induced by the supply of bioavailable dissolved
404 iron from meteoric water (Raiswell et al., 2008; Statham et al., 2008; Tonnard et al. 2018), led to a transfer of
405 DFe to the particulate phase. This is in line with the finding that around 30 % PFe had a non-lithogenic origin. In
406 addition, only 40% PMn originated from resuspended sediments. Interestingly, these two proxies remained
407 constant from the seafloor to the surface (Station 49, Figure 8), with around 25 % of the PMn of sedimentary
408 origin, which could be due to important mixing occurring on the shelf. The lithogenic PFe could result from the
409 release of PFe from Greenland bedrock captured during the ice sheet formation on land.

410 The spatial extent of the off-shelf lateral transport of particles was not important on the east Greenland coast.
411 Indeed, no visible increase of particulate trace metal concentrations was visible at the first station off-shelf, station
412 60 (Figure 8), except at 1000 m depth, where a strong increase (up to 90 %) of sedimentary PMn was seen. This
413 is probably due to the East Greenland Coastal Current (EGCC) that was located at station 53 which constrained
414 these inputs while stations 56 and 60 were under the influence of another strong current, the East Greenland-
415 Irminger current (EGIC) (Zunino et al., 2017). To the west of the Greenland margin, lateral transport of particles
416 was slightly more important. Noticeable concentrations of particulate lithogenic elements were observable until
417 station 64 located 125 km away from shoreline. These particles had a decreased PFe lithogenic contribution (50
418 %) with a similar (25 %) sedimentary PMn content than closer to the margin (Figure 8b and c). The increasing
419 nature of non-lithogenic PFe is linked to the bloom in surface waters (PFe/PAI ratio of 0.30 mol mol^{-1} , PP of 197
420 nmol L^{-1} and Chl-a concentration of 6.21 mg m^{-3} at station 61), with the gravitational settling of biogenic PFe.

421 Therefore, particles newly resuspended from Greenland sediments are an important source, representing around
422 one third of the pMn pool, combined with surface inputs such as riverine runoff and/or ice-melting that are
423 delivering particles on the shelf, and also biological production. Unlike the Iberian shelf, the Greenland margin
424 was not an important provider of particulate metals inside the Irminger and Labrador Basins, due to the circulation
425 that constrained the extent of the margin plume.

426

427

428 *The Newfoundland Shelf*

429 Previous studies have already described the influence of fresh water on the Newfoundland shelf from the Hudson
430 Strait and/or Canadian Arctic Archipelago (Fragoso et al., 2016; Yashayaev, 2007). Yashayaev (2007) also
431 monitored strong resuspension of sediments associated with the spreading of the Labrador Current along the West
432 Labrador margin.

433 Close to the Newfoundland coastline, at station 78, high fresh water discharge (≤ 32 psu) was observed in surface
434 waters (Benetti et al., 2017). Interestingly, these freshwater signatures were not associated with elevated
435 particulate trace metal concentrations. Distance of meteoric water sources implied a long travel time for the water
436 to spread through the Labrador Basin to our sampling stations. Along the journey, particles present originally may
437 have been removed from the water column by gravitational settling.

438 The proportion of lithogenic PFe was relatively high and constant throughout the water column, with a median
439 value of 70 %. At station 78, 95 % of the PMn had a sedimentary origin close to the seafloor (371 m). The
440 spreading of the recent sediment resuspension was observable until 140 m depth where the contribution of
441 sedimentary Mn was still 51% (Figure 8c, Table S2). This could correspond to an intense nepheloid layer as
442 previously reported by Biscaye and Eitrem (1977) (see also section 3.3.2). The high PFe concentration (184
443 nmol L^{-1} , station 78, 371 m depth, Figure 8b) associated with a high percentage of sedimentary PMn (95%)
444 observed at the bottom of this station, was therefore the result of an important resuspension of shelf sediments.
445 This was confirmed with low transmissometry values of 95 % (Figure 4a).

446 The important phytoplanktonic community present (maximum Chl-a= 4.91 mg m^{-3} , Tonnard et al., in prep), is
447 linked to a low PFe concentration of 0.79 nmol L^{-1} at 10 m depth, but, with a high PFe/PAI ratio, up to 0.4, and
448 PP concentration of 97 nmol L^{-1} , confirming the biological influence. Either the biogenic particles settled quickly,
449 and/or they were quickly remineralized. Concerning this latter process, intense remineralization at station 77 (7
450 $\text{mmol C m}^{-2} \text{ d}^{-1}$ compared to $4 \text{ mmol C m}^{-2} \text{ d}^{-1}$ in the Western European Basin) has been reported by Lemaitre et
451 al. (2018a and 2018b), which could explain the low PFe values throughout the water column.

452 Along the GEOVIDE section, continental shelves provided an important load of particles to the surrounding water
453 column. The three margins sampled during GEOVIDE behaved very differently; the Iberian margin discharged
454 high quantities of lithogenic particles far from the coast while the Greenland and Newfoundland margins did not
455 reveal important PFe concentrations. Spreading of particles is tightly linked to hydrodynamic conditions, which
456 in the case of the Greenland margin, prevented long distance seeding of PFe. Moreover, each margin showed a
457 specific PFe/PAI ratio (Figure 9) indicating different composition of the resuspended particles. Resuspended
458 particles represent the composition of sediment at the margin if redox transformation of iron and aluminium are
459 considered negligible under these circumstances. Differences between margins were due to the presence of non-
460 crustal particles, either biogenic or authigenic. Biological production in surface waters and authigenic formation

461 of iron hydroxide produced particles with a higher PFe/PAI content and their export through the water column to
462 the sediment increased the PFe/PAI ratio at depth. Regions where biological production is intense such as in the
463 vicinity of Newfoundland presented higher PFe/PAI ratios of resuspended benthic particles.

464

465

4.2.2 Benthic resuspended sediments

466 Along the GEOVIDE section, Benthic nepheloid layers (BNLs) provided high concentrations of particulate trace
467 elements to the deep open ocean, contributing significantly to the total budget of iron. BNLs were observable in
468 each province, although intensities varied (Figures 3 and 10).

469 In BNLs located within the WEB, PFe concentrations reached up to 10 nmol L^{-1} (stations 26 and 29, Figure 10a;
470 Table S1). These concentrations were lower than PFe concentrations in BNLs from the Icelandic (stations 32 and
471 34), Irminger (stations 42 and 44) and Labrador Basins (stations 68, 69 and 71), where benthic resuspension led
472 to PFe concentrations higher than 40 nmol L^{-1} , even reaching 89 nmol L^{-1} at the bottom of station 71 (3736 m
473 depth). Moreover, in the Irminger and Labrador Basins, PFe/PAI molar ratios within BNLs were higher than the
474 ones measured within the WEB at station 26 and 29. In the Irminger Basin, PFe/PAI reached 0.4 mol mol^{-1} (Figure
475 10b), which could reveal a mixture of lithogenic and biogenic matter that had been previously exported. This
476 feature was also observed in the Labrador Basin, with PFe/PAI ratio ranging between 0.34 and $0.44 \text{ mol mol}^{-1}$. In
477 contrast, BNLs sampled in the WEB clearly have a lithogenic imprint, with PFe/PAI molar ratios close to the
478 crustal one. Resuspended sediments with a non-crustal contribution seem to have higher PFe contents than
479 sediments with lithogenic characteristics. Nevertheless, interestingly all BNLs present during GEOVIDE were
480 spreading identically, with impacts observable up to 200 m above the oceanic seafloor (Figure 10), as reflected in
481 beam transmissometry values, and PFe concentrations, which returned to background levels at 200 m above the
482 seafloor. The presence of these BNLs has also been reported by Le Roy et al. (2018) using radium-226 activity.
483 Important differences of PFe intensities could also be due to different hydrographic components and topographic
484 characteristics. BNLs occur due to strong hydrographic stresses (i.e. boundary currents, benthic storms and deep
485 eddies) interacting with the ocean floor (Biscaye and Eittrheim, 1977; Eittrheim et al., 1976; Gardner et al., 2017,
486 2018). They are, by definition, highly variable geographically and temporally, but we have no physical data which
487 would allow us to investigate this hypothesis further.

488

489

4.2.3. Reykjanes Ridge inputs

490 Above the Reykjanes Ridge (Station 38), high PFe concentrations were determined, reaching 16 nmol L^{-1} just
491 above the seafloor, while increased DFe concentrations were reported to the east of the ridge (Tonnard et al.,
492 2018, this issue). The exact sources of iron-rich particles cannot be well constrained, as they could come from
493 active hydrothermal vents or resuspension of particulate matter from new crustal matter produced at the ridge.
494 According to the oceanic circulation (Zunino et al., 2017; Garcia-Ibanez et al., 2017), hydrothermal particles could
495 have been seen in the ISOW within the Icelandic Basin. Nevertheless, at the vicinity of the ridge, scanning electron
496 microscope (SEM) analyses of our samples did reveal several biological debris and clays but not the presence of
497 iron (oxy-)hydroxide particles (supplementary figure S1), which are known to be produced close to hydrothermal
498 vents (Elderfield and Schultz, 1996). Their absence could thus indicate an absence of vents. However, data from

499 other proxies, such as helium-3, would be necessary to confirm the presence or absence of an hydrothermal source
500 close to station 38.

501

502 4.2.4. Atmospheric inputs

503 Atmospheric deposition is an important source of trace elements in surface of the open ocean (e.g. Jickells et al.,
504 2005). Atmospheric inputs, both wet and dry, were reported to be low during the GEOVIDE cruise (Menzel
505 Barraqueta et al., 2018b, this issue; Shelley et al., 2017; 2018). In fact, oceanic particle measurements in surface
506 waters along the section did not reveal high PFe or PAI concentrations. One pattern is interesting to note: the
507 surface waters of the Iberian Abyssal Plain and Western European Basin, between stations 11 and 23 presented a
508 characteristic feature with really low PFe/PAI elemental ratios, of 0.11, smaller than the UCC ratio of 0.21 (Figure
509 6a). Such low ratios have been reported in the same region by Barrett et al. (2012). One possible explanation is
510 given by Buck et al. (2010) who described Fe-depleted aerosols in this area of the North Atlantic with PFe/PAI
511 ratio below UCC ratio. However, Shelley et al. (2017) found a higher PFe/PAI ratio around 0.25 in this area (their
512 samples geoa5-6). This result, highlights some of the difficulties in linking atmospheric inputs to water column
513 data (Baker et al., 2016), and implies a probable fractionation after aerosol deposition. In addition, there is high
514 spatial and temporal variability of atmospheric deposition (Mahowald et al., 2005) and a certain degree of
515 uncertainty about the dissolution processes of atmospherically-transported particles (Bonnet and Guieu, 2004).

516

517

518 5. Conclusions

519

520 The investigation of the PFe composition of suspended particulate matter along the GEOVIDE section in the
521 North Atlantic reflects the pervasive influence of crustal particles, augmented by sedimentary inputs at margins,
522 and within benthic nepheloid layers at depths. In consequence, variance of particulate iron along the section is
523 mainly explained by lithogenic factors.

524 Resuspension of sedimentary particles from continental shelves are responsible of high particulate iron
525 concentrations within the surrounding water column and could be observed at long distances from the shelf, in
526 the case of the Iberian margin. Our results also demonstrate the impact of Arctic meteoric water on the Greenland
527 shelf, while in surface waters, the enhancement of productivity by new bioavailable iron is leading to a transfer
528 of dissolved iron to the particulate phase. Benthic nepheloid layer are providing important concentration of
529 particles to the water column; they were observed in most of the oceanic basin encountered along the GEOVIDE
530 section.

531 Overall, PFe distributions in the North Atlantic are strongly influenced by sources at its boundaries (i.e.
532 continental margins and seafloor). When combined with other datasets from the GEOTRACES program in a
533 modelling study, for example, use of this data will facilitate a greater understanding of particulate iron cycling in
534 the North Atlantic.

535

536

537

538 **Acknowledgments**

539 We are greatly indebted to the captain and crew of the N/O Pourquoi Pas? for their help during the GEOVIDE
540 mission and clean rosette deployment. We would like to give special thanks to Fabien Péruault and Emmanuel de
541 Saint Léger for their technical expertise, to Catherine Schmechtig for the GEOVIDE database management and
542 Greg Cutter for his guidance in setting up the new French clean sampling system. We would like to thank both
543 reviewers for constructive comments that greatly improved this manuscript.

544 We also would like to thank Reiner Schlitzer for the Ocean Data View software (ODV).

545 This work was supported by the French National Research Agency (ANR-13-BS06-0014, ANR-12-PDOC-0025-
546 01), the French National Centre for Scientific Research (CNRS-LEFE-CYBER), the LabexMER (ANR-10-
547 LABX-19), and Ifremer. It was supported for the logistic by DT-INSU and GENAVIR.

548

549 **References**

550 Aguilar-Islas, A. M., Rember, R., Nishino, S., Kikuchi, T. and Itoh, M.: Partitioning and lateral transport of iron
551 to the Canada Basin, *Polar Sci.*, 7(2), 82–99, doi:10.1016/j.polar.2012.11.001, 2013.

552 Baker, A. R., Adams, C., Bell, T. G., Jickells, T. D. and Ganzeveld, L.: Estimation of atmospheric nutrient inputs
553 to the Atlantic Ocean from 50°N to 50°S based on large-scale field sampling: Iron and other dust-associated
554 elements, *Global Biogeochem. Cycles*, 27(3), 755–767, doi:10.1002/gbc.20062, 2013.

555 Baker, A. R., Landing, W. M., Bucciarelli, E., Cheize, M., Fietz, S., Hayes, C. T., Kadko, D., Morton, P. L.,
556 Rogan, N., Sarthou, G., Shelley, R. U., Shi, Z., Shiller, A. and van Hulten, M. M. P.: Trace element and isotope
557 deposition across the air–sea interface: progress and research needs, *Philos. Trans. R. Soc. A Math. Phys. Eng.*
558 *Sci.*, 374(2081), 20160190, doi:10.1098/rsta.2016.0190, 2016.

559 Barrett, P. M., Resing, J. A., Buck, N. J., Buck, C. S., Landing, W. M. and Measures, C. I.: The trace element
560 composition of suspended particulate matter in the upper 1000m of the eastern North Atlantic Ocean: A16N, *Mar.*
561 *Chem.*, 142–144, 41–53, doi:10.1016/j.marchem.2012.07.006, 2012.

562 Benetti, M., Reverdin, G., Lique, C., Yashayaev, I., Holliday, N. P., Tynan, E., Torres-Valdes, S., Lherminier, P.,
563 Tréguer, P., and Sarthou, G.: Composition of freshwater in the spring of 2014 on the southern Labrador shelf and
564 slope, *Journal of Geophysical Research: Oceans*, 122, 1102–1121, 10.1002/2016jc012244, 2017.

565 Berger, C. J. M., Lippiatt, S. M., Lawrence, M. G. and Bruland, K. W.: Application of a chemical leach technique
566 for estimating labile particulate aluminum, iron, and manganese in the Columbia River plume and coastal waters
567 off Oregon and Washington, *J. Geophys. Res.*, 113, C00B01, doi:10.1029/2007JC004703, 2008.

568 Bergquist, B. A., Wu, J. and Boyle, E. A.: Variability in oceanic dissolved iron is dominated by the colloidal
569 fraction, *Geochim. Cosmochim. Acta*, 71(12), 2960–2974, doi:10.1016/j.gca.2007.03.013, 2007.

570 Bhatia, M. P., Kujawinski, E. B., Das, S. B., Breier, C. F., Henderson, P. B. and Charette, M. A.: Greenland
571 meltwater as a significant and potentially bioavailable source of iron to the ocean, *Nat. Geosci.*, 6(4), 274–278,
572 doi:10.1038/ngeo1746, 2013.

573 Biscaye, P. E. and Eitrem, S. L.: Suspended Particulate Loads and Transports in the Nepheloid Layer of the
574 Abyssal Atlantic Ocean, *Dev. Sedimentol.*, 23(C), 155–172, doi:10.1016/S0070-4571(08)70556-9, 1977.

575 Bishop, J. K. B. and Biscaye, P. E.: Chemical characterization of individual particles from the nepheloid layer in
576 the Atlantic Ocean, *Earth Planet. Sci. Lett.*, 58(2), 265–275, doi:10.1016/0012-821X(82)90199-6, 1982.

577 Bishop, J. K. B. and Fleisher, M. Q.: Particulate manganese dynamics in Gulf Stream warm-core rings and
578 surrounding waters of the N.W. Atlantic, *Geochim. Cosmochim. Acta*, 51(10), 2807–2825, doi:10.1016/0016-
579 7037(87)90160-8, 1987.

580 Bonnet, S. and Guieu C.: Dissolution of atmospheric iron in seawater, *Geophys. Res. Lett.*, 31(3), L03303,
581 doi:10.1029/2003GL018423, 2004.

582 Boyle, E. A., Bergquist, B. A., Kayser, R. A. and Mahowald, N.: Iron, manganese, and lead at Hawaii Ocean
583 Time-series station ALOHA: Temporal variability and an intermediate water hydrothermal plume, *Geochim.*
584 *Cosmochim. Acta*, 69(4), 933–952, doi:10.1016/j.gca.2004.07.034, 2005.

585 Buck, C. S., Landing, W. M., Resing, J. A. and Measures, C. I.: The solubility and deposition of aerosol Fe and
586 other trace elements in the North Atlantic Ocean: Observations from the A16N CLIVAR/CO2repeat hydrography
587 section, *Mar. Chem.*, 120(1–4), 57–70, doi:10.1016/j.marchem.2008.08.003, 2010.

588 Cheize, M., Planquette, H. F., Fitzsimmons, J. N., Pelleter, E., Sherrell, R. M., Lambert, C., Bucciarelli, E.,
589 Sarthou, G., Le Goff, M., Liorzou, C., Chéron, S., Viollier, E., and Gayet, N.: Contribution of resuspended
590 sedimentary particles to dissolved iron and manganese in the ocean: An experimental study, *Chemical Geology*.
591 doi: 10.1016/j.chemgeo.2018.10.003, 2018.

592 Collier, R. and Edmond, J.: The trace element geochemistry of marine biogenic particulate matter, *Prog.*
593 *Oceanogr.*, 13(2), 113–199, doi:10.1016/0079-6611(84)90008-9, 1984.

594 Cullen, J. T., Chong, M. and Ianson, D.: British columbia continental shelf as a source of dissolved iron to the
595 subarctic northeast Pacific Ocean, *Global Biogeochem. Cycles*, 23(4), 1–12, doi:10.1029/2008GB003326, 2009.

596 Cutter, G. A. and Bruland, K. W.: Rapid and noncontaminating sampling system for trace elements in global
597 ocean surveys, *Limnol. Oceanogr. Methods*, 10(JUNE), 425–436, doi:10.4319/lom.2012.10.425, 2012.

598 Dammshäuser, A., Wagener, T., Garbe-Schönberg, D. and Croot, P.: Particulate and dissolved aluminum and
599 titanium in the upper water column of the Atlantic Ocean, *Deep. Res. Part I Oceanogr. Res. Pap.*, 73, 127–139,
600 doi:10.1016/j.dsr.2012.12.002, 2013.

601 Dehairs, F., Jacquet, S., Savoye, N., Van Mooy, B. A. S., Buesseler, K. O., Bishop, J. K. B., Lamborg, C. H.,
602 Elskens, M., Baeyens, W., Boyd, P. W., Casciotti, K. L. and Monnin, C.: Barium in twilight zone suspended
603 matter as a potential proxy for particulate organic carbon remineralization: Results for the North Pacific, *Deep.*
604 *Res. Part II Top. Stud. Oceanogr.*, 55(14–15), 1673–1683, doi:10.1016/j.dsr2.2008.04.020, 2008.

605 Dutay, J. C., Tagliabue, A., Kriest, I. and van Hulst, M. M. P.: Modelling the role of marine particles on large
606 scale ^{231}Pa , ^{230}Th , Iron and Aluminium distributions, *Prog. Oceanogr.*, 133, 66–72,
607 doi:10.1016/j.pocean.2015.01.010, 2015.

608 Eitner, S., Thorndike, E. M. and Sullivan, L.: Turbidity distribution in the Atlantic Ocean, *Deep. Res. Oceanogr.*
609 *Abstr.*, 23(12), 1115–1127, doi:10.1016/0011-7471(76)90888-3, 1976.

610 Elderfield, H. and Schultz, A.: Mid-Ocean Ridge Hydrothermal Fluxes and the Chemical Composition of the
611 Ocean, *Annu. Rev. Earth Planet. Sci.*, 24(1), 191–224, doi:10.1146/annurev.earth.24.1.191, 1996.

612 Ellwood, M. J., Nodder, S. D., King, A. L., Hutchins, D. A., Wilhelm, S. W. and Boyd, P. W.: Pelagic iron cycling
613 during the subtropical spring bloom, east of New Zealand, *Mar. Chem.*, 160, 18–33,
614 doi:10.1016/j.marchem.2014.01.004, 2014.

615 Elrod, V. A., Berelson, W. M., Coale, K. H. and Johnson, K. S.: The flux of iron from continental shelf sediments:
616 A missing source for global budgets, *Geophys. Res. Lett.*, 31(12), 2–5, doi:10.1029/2004GL020216, 2004.

617 Fitzwater, S. E., Johnson, K. S., Gordon, R. M., Coale, K. H. and Smith, W. O.: Trace metal concentrations in
618 the Ross Sea and their relationship with nutrients and phytoplankton growth, *Deep. Res. Part II Top. Stud.*
619 *Oceanogr.*, 47(15–16), 3159–3179, doi:10.1016/S0967-0645(00)00063-1, 2000.

620 Fragoso, G. M., Poulton, A. J., Yashayaev, I. M., Head, E. J. H., Stinchcombe, M. C. and Purdie, D. A.:
621 Biogeographical patterns and environmental controls of phytoplankton communities from contrasting
622 hydrographical zones of the Labrador Sea, *Prog. Oceanogr.*, 141, 212–226, doi:10.1016/j.pocean.2015.12.007,
623 2016.

624 Frew, R. D., Hutchins, D. A., Nodder, S., Sanudo-Wilhelmy, S., Tovar-Sanchez, A., Leblanc, K., Hare, C. E. and
625 Boyd, P. W.: Particulate iron dynamics during FeCycle in subantarctic waters southeast of New Zealand, *Global*
626 *Biogeochem. Cycles*, 20(1), 1–15, doi:10.1029/2005GB002558, 2006.

627 García-Ibáñez, M. I., Pardo, P. C., Carracedo, L. I., Mercier, H., Lherminier, P., Ríos, A. F. and Pérez, F. F.:
628 Structure, transports and transformations of the water masses in the Atlantic Subpolar Gyre, *Prog. Oceanogr.*, 135,
629 18–36, doi:10.1016/j.pocean.2015.03.009, 2015.

630 Gardner, W. D., Tucholke, B. E., Richardson, M. J. and Biscaye, P. E.: Benthic storms, nepheloid layers, and
631 linkage with upper ocean dynamics in the western North Atlantic, *Mar. Geol.*, 385, 304–327,
632 doi:10.1016/j.margeo.2016.12.012, 2017.

633 Gardner, W. D., Richardson, M. J. and Mishonov, A. V.: Global assessment of benthic nepheloid layers and
634 linkage with upper ocean dynamics, *Earth Planet. Sci. Lett.*, 482, 126–134, doi:10.1016/j.epsl.2017.11.008, 2018.

635 Gerringa, L. J. A., Rijkenberg, M. J. A., Schoemann, V., Laan, P. and de Baar, H. J. W.: Organic complexation
636 of iron in the West Atlantic Ocean, *Mar. Chem.*, 177, 434–446, doi:10.1016/j.marchem.2015.04.007, 2015.

637 Hawkings, J. R., Wadham, J. L., Tranter, M., Raiswell, R., Benning, L. G., Statham, P. J., Tedstone, A., Nienow,
638 P., Lee, K. and Telling, J.: Ice sheets as a significant source of highly reactive nanoparticulate iron to the oceans,
639 *Nat. Commun.*, 5(May), 1–8, doi:10.1038/ncomms4929, 2014.

640 Hwang, J., Druffel, E. R. M. and Eglinton, T. I.: Widespread influence of resuspended sediments on oceanic
641 particulate organic carbon: Insights from radiocarbon and aluminum contents in sinking particles, *Global*
642 *Biogeochem. Cycles*, 24(4), 1–10, doi:10.1029/2010GB003802, 2010.

643 Jeandel, C. and Oelkers, E. H.: The influence of terrigenous particulate material dissolution on ocean chemistry
644 and global element cycles, *Chem. Geol.*, 395, 50–66, doi:10.1016/j.chemgeo.2014.12.001, 2015.

645 Jeandel, C., Peucker-Ehrenbrink, B., Jones, M. T., Pearce, C. R., Oelkers, E. H., Godderis, Y., Lacan, F., Aumont,
646 O. and Arsouze, T.: Ocean margins: The missing term in oceanic element budgets?, *Eos, Transactions American*
647 *Geophysical Union*, 92(26), 217–224, doi: 10.1029/2011EO260001, 2011.

648 Jickells, T. D., An, Z. S., Andersen, K. K., Baker, A. R., Bergametti, C., Brooks, N., Cao, J. J., Boyd, P. W., Duce,
649 R. A., Hunter, K. A., Kawahata, H., Kubilay, N., LaRoche, J., Liss, P. S., Mahowald, N., Prospero, J. M.,
650 Ridgwell, A. J., Tegen, I. and Torres, R.: Global iron connections between desert dust, ocean biogeochemistry,
651 and climate, *Science (80-.)*, 308(5718), 67–71, doi:10.1126/science.1105959, 2005.

652 Jouanneau, J. M., Garcia, C., Oliveira, A., Rodrigues, A., Dias, J. A. and Weber, O.: Dispersal and deposition of
653 suspended sediment on the shelf off the Tagus and Sado estuaries, S.W. Portugal, *Prog. Oceanogr.*, 42(1–4), 233–
654 257, doi:10.1016/S0079-6611(98)00036-6, 1998.

655 Labatut, M., Lacan, F., Pradoux, C., Chmeleff, J., Radic, A., Murray, J. W., Poitrasson, F., Johansen, A. M., Thil,
656 F., Lacan, F., Pradoux, C., Chmeleff, J., Radic, A., Murray, J. W., Poitrasson, F., Johansen, A. M. and Thil, F.:
657 Iron sources and dissolved-particulate interactions in the seawater of the Western Equatorial Pacific, iron isotope
658 perspectives., *Global Biogeochem Cycles*, 1044–1065, doi:10.1002/2014GB004928, 2014.

659 Lam, P. J. and Bishop, J. K. B.: The continental margin is a key source of iron to the HNLC North Pacific Ocean,
660 *Geophys. Res. Lett.*, 35(7), 1–5, doi:10.1029/2008GL033294, 2008.

661 Lam, P. J., Ohnemus, D. C. and Marcus, M. A.: The speciation of marine particulate iron adjacent to active and
662 passive continental margins, *Geochim. Cosmochim. Acta*, 80, 108–124, doi:10.1016/j.gca.2011.11.044, 2012.

663 Lam, P. J., Ohnemus, D. C. and Auro, M. E.: Size-fractionated major particle composition and concentrations
664 from the US GEOTRACES North Atlantic Zonal Transect, *Deep. Res. Part II Top. Stud. Oceanogr.*, 116, 303–
665 320, doi:10.1016/j.dsr2.2014.11.020, 2015.

666 Lam, P. J., Lee, J. M., Heller, M. I., Mehic, S., Xiang, Y. and Bates, N. R.: Size-fractionated distributions of
667 suspended particle concentration and major phase composition from the U.S. GEOTRACES Eastern Pacific Zonal
668 Transect (GP16), *Mar. Chem.*, (April), 0–1, doi:10.1016/j.marchem.2017.08.013, 2017.

669 Lannuzel, D., Bowie, A. R., van der Merwe, P. C., Townsend, A. T. and Schoemann, V.: Distribution of dissolved
670 and particulate metals in Antarctic sea ice, *Mar. Chem.*, 124(1–4), 134–146, doi:10.1016/j.marchem.2011.01.004,
671 2011.

672 Lannuzel, D., Van der Merwe, P. C., Townsend, A. T. and Bowie, A. R.: Size fractionation of iron, manganese
673 and aluminium in Antarctic fast ice reveals a lithogenic origin and low iron solubility, *Mar. Chem.*, 161, 47–56,
674 doi:10.1016/j.marchem.2014.02.006, 2014.

675 Lee, J. M., Heller, M. I. and Lam, P. J.: Size distribution of particulate trace elements in the U.S. GEOTRACES
676 Eastern Pacific Zonal Transect (GP16), *Mar. Chem.*, 201(September 2017), 108–123,
677 doi:10.1016/j.marchem.2017.09.006, 2017.

678 Lemaître, N., planquette, H., Planchon, F., Sarthou, G., Jacquet, S., Garcia-Ibanez, M. I., Gourain, A., Cheize,
679 M., Monin, L., Andre, L., Laha, P., Terryn, H., and Dehairs, F.: Particulate barium tracing significant mesopelagic
680 carbon remineralisation in the North Atlantic, *Biogeosciences*, doi:10.5194/bg-15-2289-2018, 2018a.

681 Lemaître, N., Planchon, F., Planquette, H., Dehairs, F., Fonseca-Batista, D., Roukaerts, A., Deman, F., Tang, Y.,
682 Mariez, C., and Sarthou G.: High variability of export fluxes along the North Atlantic GEOTRACES section
683 GA01: Particulate organic carbon export deduced from the ^{234}Th method, *Biogeosciences*, doi:10.5194/bg-2018-
684 190, 2018b.

685 Le Roy, E., Sanial, V., Charette, M.A., Van Beek, P., Lacan, F., Jacquet, S.H., Henderson, P.B., Souhaut, M.,
686 García-Ibáñez, M.I., Jeandel, C. and Pérez, F.: The ^{226}Ra -Ba relationship in the North Atlantic during
687 GEOTRACES-GA01, *Biogeosciences*, doi:10.5194/bg-2017-478, 2018.

688 Marsay, C. M., Lam, P. J., Heller, M. I., Lee, J. M. and John, S. G.: Distribution and isotopic signature of ligand-
689 leachable particulate iron along the GEOTRACES GP16 East Pacific Zonal Transect, *Mar. Chem.*, (November
690 2016), 1–14, doi:10.1016/j.marchem.2017.07.003, 2017.

691 Martin, J. H., Fitzwater, S. E., Michael Gordon, R., Hunter, C. N. and Tanner, S. J.: Iron, primary production and
692 carbon-nitrogen flux studies during the JGOFS North Atlantic bloom experiment, *Deep. Res. Part II*, 40(1–2),
693 115–134, doi:10.1016/0967-0645(93)90009-C, 1993.

694 McCave, I. N. and Hall, I. R.: Turbidity of waters over the Northwest Iberian continental margin, *Prog. Oceanogr.*,
695 52(2–4), 299–313, doi:10.1016/S0079-6611(02)00012-5, 2002.

696 Menzel Barraqueta, J.L., Schlosser, C., Planquette, H., Gourain, A., Cheize, M., Boutorh, J., Shelley, R., Pereira
697 Contreira, L., Gledhill, M., Hopwood, M.J. and Lherminier, P.: Aluminium in the North Atlantic Ocean and the
698 Labrador Sea (GEOTRACES GA01 section): roles of continental inputs and biogenic particle removal.
699 *Biogeosciences*, 1-28, doi: 10.5194/bg-2018-39, 2018.

700

701 Menzel Barraqueta, J.-L., Klar, J. K., Gledhill, M., Schlosser, C., Shelley, R., Planquette, H., Wenzel, B.,
702 Sarthou, G., and Achterberg, E. P.: Atmospheric aerosol deposition fluxes over the Atlantic Ocean: A
703 GEOTRACES case study, *Biogeosciences Discuss.*, <https://doi.org/10.5194/bg-2018-209>, in review, 2018b.

704 Milne, A., Schlosser, C., Wake, B. D., Achterberg, E. P., Chance, R., Baker, A. R., Forryan, A. and Lohan, M.
705 C.: Particulate phases are key in controlling dissolved iron concentrations in the (sub)tropical North Atlantic,
706 *Geophys. Res. Lett.*, 44(5), 2377–2387, doi:10.1002/2016GL072314, 2017.

707 Nuester, J., Shema, S., Vermont, A., Fields, D. M. and Twining, B. S.: The regeneration of highly bioavailable
708 iron by meso- and microzooplankton, *Limnol Oceanogr.*, 59(4), 1399–1409, doi:10.4319/lom.2014.59.4.1399, 2014.

709 Oelkers, E. H., Jones, M. T., Pearce, C. R., Jeandel, C., Eiriksdottir, E. S. and Gislason, S. R.: Riverine particulate
710 material dissolution in seawater and its implications for the global cycles of the elements, *Geosci.*, 344(11–12),
711 646–651, doi:10.1016/j.crte.2012.08.005, 2012.

712 Ohnemus, D. C. and Lam, P. J.: Cycling of lithogenic marine particles in the US GEOTRACES North Atlantic
713 transect, *Deep. Res. Part II Top. Stud. Oceanogr.*, 116, 283–302, doi:10.1016/j.dsr2.2014.11.019, 2015.

714 Peers, G. and Price, N. M.: A role for manganese in superoxide dismutases and growth of iron-deficient diatoms,
715 *Limnol. Oceanogr.*, 49(5), 1774–1783, doi:10.4319/lom.2004.49.5.1774, 2004.

716 Planquette, H. and Sherrell, R. M.: Sampling for particulate trace element determination using water sampling
717 bottles: Methodology and comparison to in situ pumps, *Limnol. Oceanogr. Methods*, 10(5), 367–388,
718 doi:10.4319/lom.2012.10.367, 2012.

719 Planquette, H., Fones, G. R., Statham, P. J. and Morris, P. J.: Origin of iron and aluminium in large particles (>
720 53 μm) in the Crozet region, Southern Ocean, *Mar. Chem.*, 115(1–2), 31–42, doi:10.1016/j.marchem.2009.06.002,
721 2009.

722 Planquette, H., Sanders, R. R., Statham, P. J., Morris, P. J. and Fones, G. R.: Fluxes of particulate iron from the
723 upper ocean around the Crozet Islands: A naturally iron-fertilized environment in the Southern Ocean, *Global*
724 *Biogeochem. Cycles*, 25(2), doi:10.1029/2010GB003789, 2011.

725 Planquette, H., Sherrell, R. M., Stammerjohn, S. and Field, M. P.: Particulate iron delivery to the water column
726 of the Amundsen Sea, Antarctica, *Mar. Chem.*, 153, 15–30, doi:10.1016/j.marchem.2013.04.006, 2013.

727 Radic, A., Lacan, F. and Murray, J. W.: Iron isotopes in the seawater of the equatorial Pacific Ocean: New
728 constraints for the oceanic iron cycle, *Earth Planet. Sci. Lett.*, 306(1–2), 1–10, doi:10.1016/j.epsl.2011.03.015,
729 2011.

730 Raiswell, R., Benning, L. G., Tranter, M. and Tulaczyk, S.: Bioavailable iron in the Southern Ocean: The
731 significance of the iceberg conveyor belt, *Geochem. Trans.*, 9(1), 7, doi:10.1186/1467-4866-9-7, 2008.

732 Rijkenberg, M. J. A., Middag, R., Laan, P., Gerringa, L. J. A., Van Aken, H. M., Schoemann, V., De Jong, J. T.
733 M. and De Baar, H. J. W.: The distribution of dissolved iron in the West Atlantic Ocean, PLoS One, 9(6), 1–14,
734 doi:10.1371/journal.pone.0101323, 2014.

735 Sanders, R., Henson, S. A., Koski, M., De La Rocha, C. L., Painter, S. C., Poulton, A. J., Riley, J., Salihoglu, B.,
736 Visser, A., Yool, A., Bellerby, R. and Martin, A. P.: The Biological Carbon Pump in the North Atlantic, Prog.
737 Oceanogr., 129(PB), 200–218, doi:10.1016/j.pocean.2014.05.005, 2014.

738 Sarthou, G., Lherminier, and the GEOVIDE team: Introduction to the French GEOTRACES North Atlantic
739 Transect (GA01): GEOVIDE cruise, Biogeosciences, 15, 7097–7109, <https://doi.org/10.5194/bg-15-7097-2018>,
740 2018.

741 Sarthou, G., Vincent, D., Christaki, U., Obernosterer, I., Timmermans, K. R. and Brussaard, C. P. D.: The fate of
742 biogenic iron during a phytoplankton bloom induced by natural fertilisation: Impact of copepod grazing, Deep.
743 Res. Part II Top. Stud. Oceanogr., 55(5–7), 734–751, doi:10.1016/j.dsr2.2007.12.033, 2008.

744 Schlosser, C., Schmidt, K., Aquilina, A., Homoky, W. B., Castrillejo, M., Mills, R. A., Patey, M. D., Fielding, S.,
745 Atkinson, A. and Achterberg, E. P.: Mechanisms of dissolved and labile particulate iron supply to shelf waters
746 and phytoplankton blooms off South Georgia, Southern Ocean, Biogeosciences, 15, 4973–4993, doi: 10.5194/bg-
747 15-4973-2018, 2018.

748 Shelley, R. U., Landing, W. M., Ussher, S. J., Planquett, H. and Sarthou, G.: Characterisation of aerosol
749 provenance from the fractional solubility of Fe (Al, Ti, Mn, Co, Ni, Cu, Zn, Cd and Pb) in North Atlantic aerosols
750 (GEOTRACES GA01 and GA03), Biogeosciences, 15, 2271–2288, doi: 10.5194/bg-15-2271-2018, 2018

751 Shelley, R. U., Landing, W. M., Ussher, S. J., Planquette, H. and Sarthou, G.: Regional trends in the fractional
752 solubility of Fe and other metals from North Atlantic aerosols (GEOTRACES cruises GA01 and GA03) following
753 a two-stage leach, Biogeosciences, 15(1), 2271–2288, doi:10.5194/bg-15-2271-2018, 2018.

754 Sherrell, R. M., Field, P. M. and Gao, Y.: Temporal variability of suspended mass and composition in the
755 Northeast Pacific water column: Relationships to sinking flux and lateral advection, Deep. Res. Part II Top. Stud.
756 Oceanogr., 45(4–5), 733–761, doi:10.1016/S0967-0645(97)00100-8, 1998.

757 Spinrad, R. W., Zaneveld, J. R. and Kitchen, J. C.: A Study of the Optical Characteristics of the Suspended Particles
758 Benthic Nepheloid Layer of the Scotian Rise, J. Geophys. Res., 88, 7641–7645, doi:10.1029/83J003C, 1983.

759 Statham, P. J., Skidmore, M. and Tranter, M.: Inputs of glacially derived dissolved and colloidal iron to the coastal
760 ocean and implications for primary productivity, Global Biogeochem. Cycles, 22(3), 1–11,
761 doi:10.1029/2007GB003106, 2008.

762 Straneo, F., Pickart, R. S. and Lavender, K.: Spreading of Labrador sea water: An advective-diffusive study based
763 on Lagrangian data, Deep. Res. Part I Oceanogr. Res. Pap., 50(6), 701–719, doi:10.1016/S0967-0637(03)00057-
764 8, 2003.

- 765 Sunda, W. G. and Huntsman, S. A.: Effect of Competitive Interactions Between Manganese and Copper on
766 Cellular Manganese and Growth in Estuarine and Oceanic Species of the Diatom *Thalassiosira*, *Limnol.*
767 *Oceanogr.*, 28(5), 924–934, doi:10.4319/lo.1983.28.5.0924, 1983.
- 768 Tagliabue, A., Bopp, L., Dutay, J. C., Bowie, A. R., Chever, F., Jean-Baptiste, P., Bucciarelli, E., Lannuzel, D.,
769 Remenyi, T., Sarthou, G., Aumont, O., Gehlen, M. and Jeandel, C.: Hydrothermal contribution to the oceanic
770 dissolved iron inventory, *Nat. Geosci.*, 3(4), 252–256, doi:10.1038/ngeo818, 2010.
- 771 Tagliabue, A., Bowie, A. R., Boyd, P. W., Buck, K. N., Johnson, K. S. and Saito, M. A.: The integral role of iron
772 in ocean biogeochemistry, *Nature*, 543(7643), 51–59, doi:10.1038/nature21058, 2017.
- 773 Taylor, S. and McLennan, S.: The geochemical evolution of the continental crust, *Rev. Geophys.*, 33(2), 241–
774 265, doi:10.1029/95RG00262, 1995.
- 775 Tebo, B. M. and Emerson, S. R.: Effect of Oxygen Tension Manganese (II) Concentration and Temperature on
776 the Microbially Catalyzed Manganese-Ii Oxidation Rate in a Marine Fjord, *Appl. Environ. Microbiol.*, 50(5),
777 1268–1273, 1985.
- 778 Tebo, B. M., Neelson, K. H., Emerson, S. and Jacobs, L.: Microbial mediation of Mn(II) and Co(II) precipitation
779 at the o₂/H₂S interfaces in two anoxic fjords, 29(6), 1247–1258, 1984.
- 780 Tonnard, M., Planquette, H., Bowie, A. R., van der Merwe, P., Gallinari, M., Desprez de Gésincourt, F., Germain,
781 Y., Gourain, A., Benetti, M., Reverdin, G., Tréguer, P., Boutorh, J., Cheize, M., Menzel Barraqueta, J.L., Pereira-
782 Contreira, L., Shelley, R., Lherminier, P., and Sarthou, G.: Dissolved iron in the North Atlantic Ocean and
783 Labrador Sea along the GEOVIDE section (GEOTRACES section GA01), *Biogeosciences Discuss.*,
784 <https://doi.org/10.5194/bg-2018-147>, 2018
- 785 Trefry, J. H., Trocine, R. P., Klinkhammer, G. P. and Rona, P. A.: Iron and copper enrichment of suspended
786 particles in dispersed hydrothermal plumes along the mid-Atlantic Ridge, *Geophys. Res. Lett.*, 12(8), 506–509,
787 doi:10.1029/GL012i008p00506, 1985.
- 788 Ussher, S. J., Achterberg, E. P. and Worsfold, P. J.: Marine biogeochemistry of iron, *Environ. Chem.*, 1(2), 67–
789 80, doi:10.1071/EN04053, 2004.
- 790 Ussher, S. J., Worsfold, P. J., Achterberg, E. P., Laëis, A., Blain, S., Laan, P., de Baar, H. J. W.: Distribution and
791 redox speciation of dissolved iron on the European continental margin, *Limnol. Oceanogr.*, 52(6), 2530–2539,
792 doi:10.4319/lo.2007.52.6.2530, 2007.
- 793 Van der Merwe, P., Lannuzel, D., Bowie, A. R., Mancuso Nichols, C. A. and Meiners, K. M.: Iron fractionation
794 in pack and fast ice in East Antarctica: Temporal decoupling between the release of dissolved and particulate iron
795 during spring melt, *Deep. Res. Part II Top. Stud. Oceanogr.*, 58(9–10), 1222–1236,
796 doi:10.1016/j.dsr2.2010.10.036, 2011a.

797 Van Der Merwe, P., Lannuzel, D., Bowie, A. R. and Meiners, K. M.: High temporal resolution observations of
798 spring fast ice melt and seawater iron enrichment in East Antarctica, *J. Geophys. Res. Biogeosciences*, 116(3), 1–
799 18, doi:10.1029/2010JG001628, 2011b.

800 Weinstein, S. E. and Moran, S. B.: Distribution of size-fractionated particulate trace metals collected by bottles
801 and in-situ pumps in the Gulf of Maine-Scotian Shelf and Labrador Sea, *Mar. Chem.*, 87(3–4), 121–135,
802 doi:10.1016/j.marchem.2004.02.004, 2004.

803 Yashayaev, I.: Hydrographic changes in the Labrador Sea, 1960-2005, *Prog. Oceanogr.*, 73(3–4), 242–276,
804 doi:10.1016/j.pocean.2007.04.015, 2007.

805 Yashayaev, I. and Loder, J. W.: Enhanced production of Labrador Sea Water in 2008, *Geophys. Res. Lett.*, 36(1),
806 doi:10.1029/2008GL036162, 2009.

807 Zunino, P., Lherminier, P., Mercier, H., Daniault, N., García-Ibáñez, M. I., and Pérez, F. F.: The GEOVIDE
808 cruise in May–June 2014 reveals an intense Meridional Overturning Circulation over a cold and fresh subpolar
809 North Atlantic. *Biogeosciences*, 14(23), 5323, 2017.

810

811

812

813

814

815

816

817

818

819

820

821

822

823

824

825

826

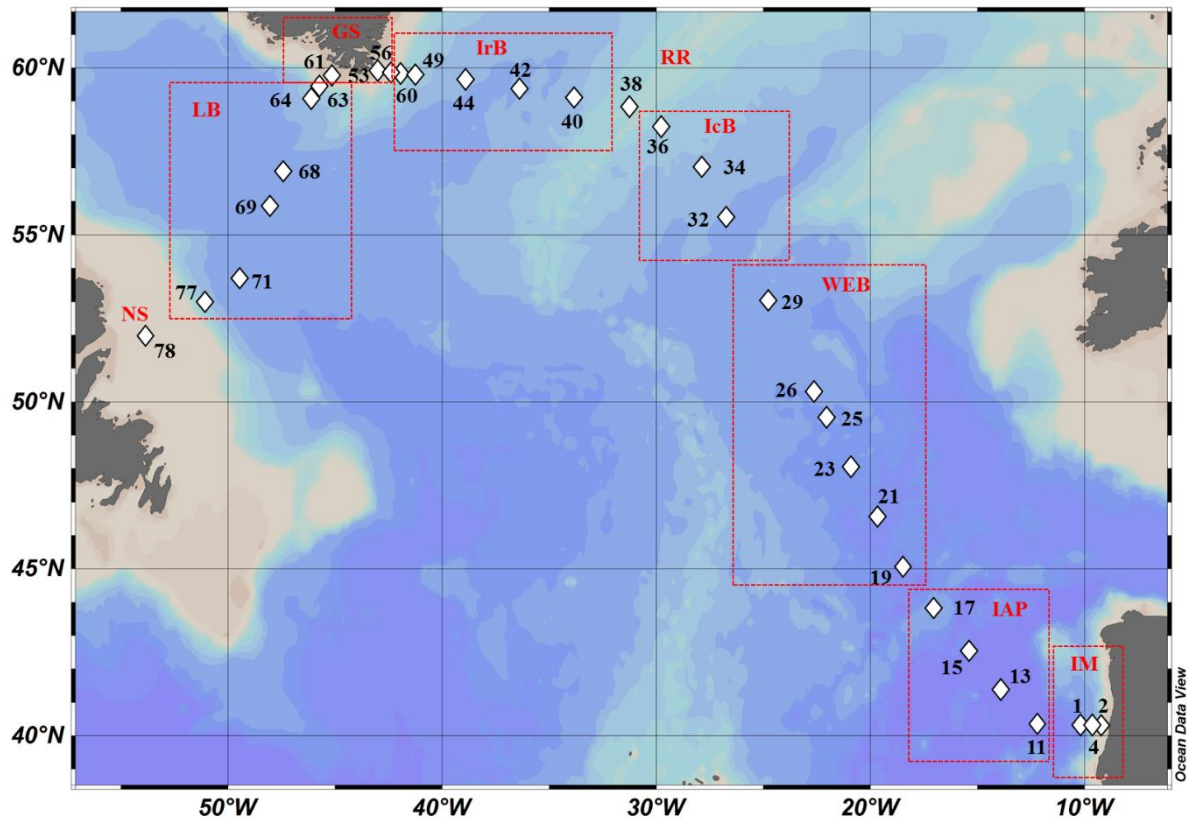
827

828

829

830

831 **Figure 1: Map of stations where suspended particle samples were collected with GO-FLO bottles during the GEOVIDE**
832 **cruise (GA01) in the North Atlantic Ocean. Biogeochemical provinces are indicated by red squares, IM: Iberian**
833 **Margin, IAP: Iberian Abyssal Plain, WEB: Western European Basin, IcB: Iceland Basin, RR: Reykjanes Ridge, IrB:**
834 **Irminger Basin, GS: Greenland Shelf, LB: Labrador Basin, NS: Newfoundland Shelf. This figure was generated using**
835 **Ocean Data View (Schlitzer, R., Ocean Data View, odv.awi.de, 2017).**



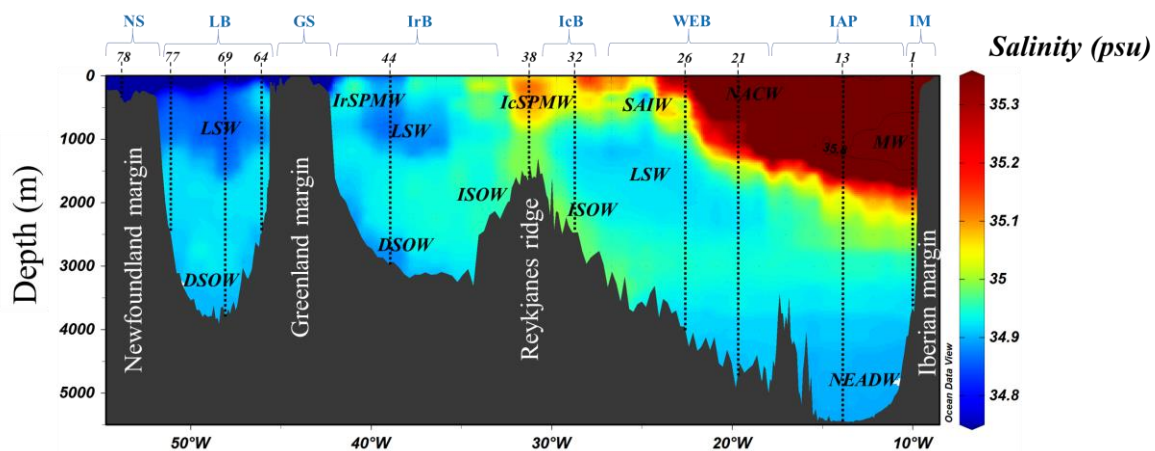
836
 837
 838
 839
 840
 841
 842
 843
 844
 845
 846
 847
 848
 849
 850
 851

852 **Figure 2: Salinity section during the GEOVIDE cruise with water masses indicated in black italic font. A salinity**
 853 **contour of 35.8 psu have been applied to identify the Mediterranean Water (MW) to the east. From right to left; North**
 854 **East Atlantic Deep Water (NEADW); North Atlantic Central Water (NACW); Labrador Sea Water (LSW); Sub-**
 855 **Arctic Intermediate Water (SAIW); Iceland-Scotland Overflow Water (ISOW); Iceland Sub-Polar Mode Water**
 856 **(IcSPMW); Denmark Strait Overflow Water (DSOW); Irminger Sub-Polar Mode Water (IrSPMW).** Station locations

857 are indicated by the numbers above the section and biogeochemical provinces are indicated in blue font above station
858 numbers. This figure was generated using Ocean Data View (Schlitzer, R., Ocean Data View, odv.awi.de, 2017).

859

860



861

862

863

864

865

866

867

868

869

870

871

872

873

874

875

876

877

878

879

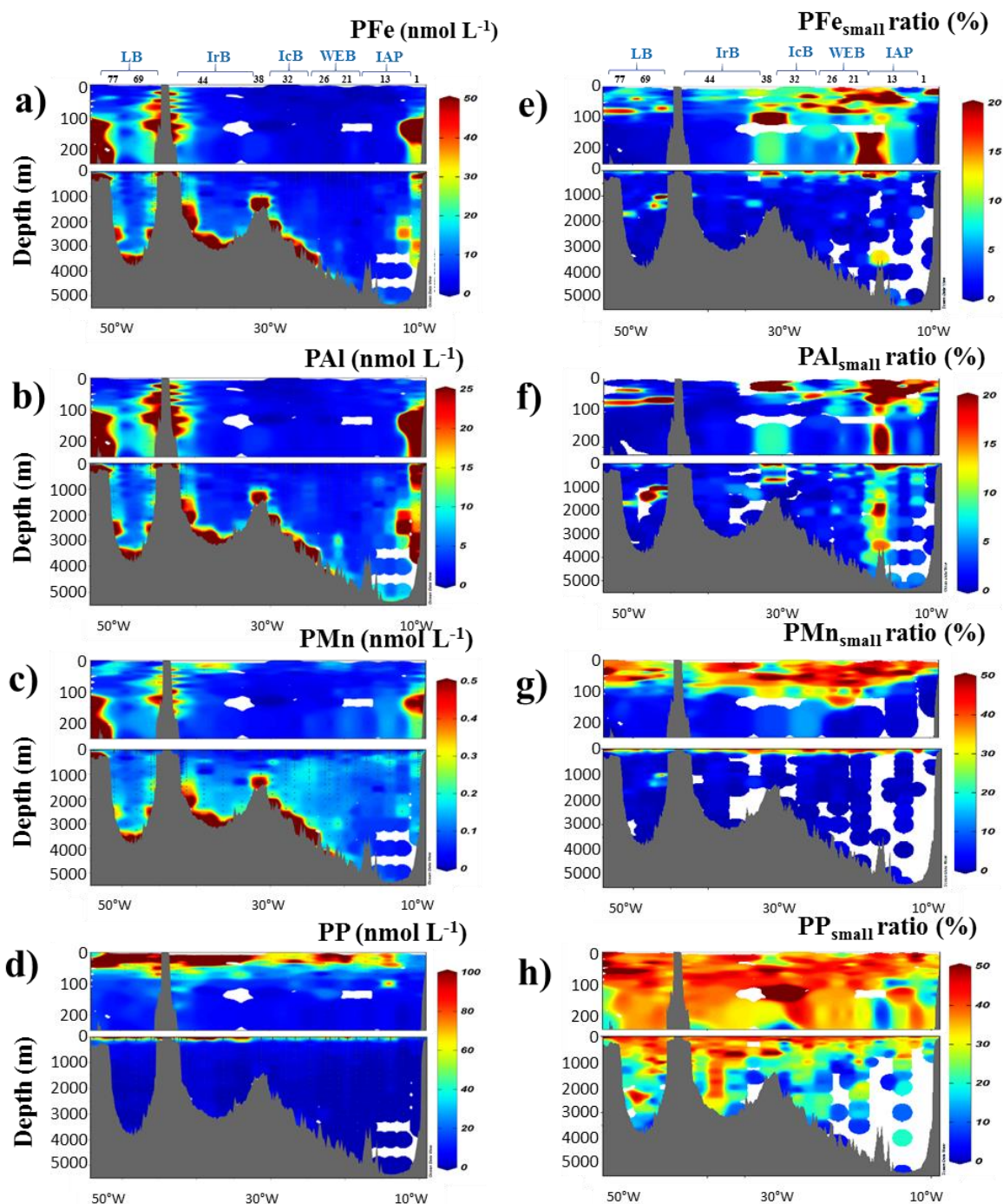
880

881

882 **Figure 3:** Left panel: Distribution of total particulate (a) iron (PFe), (b) aluminium (PAI), (c) manganese (PMn) and
883 (d) phosphorus (PP) concentrations (nmol L^{-1}) in the first 250 m and the entire water column along the GEOVIDE
884 section in the North Atlantic Ocean. Right panel: Contribution of the small size fraction ($0.45\text{-}5\ \mu\text{m}$) expressed as a
885 percentage (%) of the total concentration of (e) PFe, (f) PAI, (g) PMn and (h) PP. Station IDs and biogeochemical

886
887

regions are indicated on top of sections a and e. This figure was generated using Ocean Data View (Schlitzer, R., Ocean Data View, odv.awi.de, 2017).



888

889

890

891

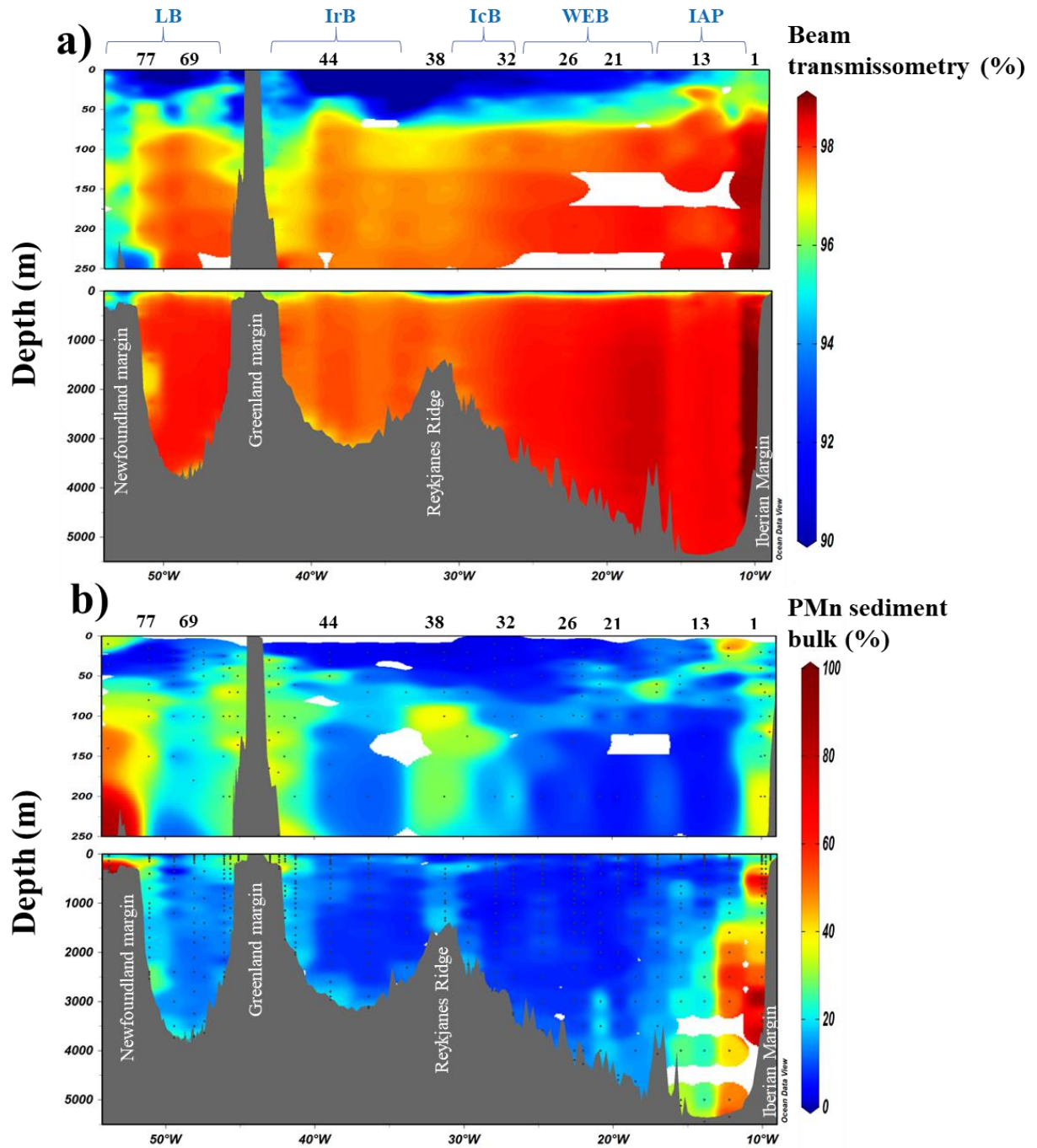
892

893

894

895

Figure 4: Section of derived contributions of sedimentary inputs along the GA01 section with (a) beam transmissometry (%) and (b) manganese bulk sediment proxy (%) based on Eq (3). Station IDs and biogeochemical region are indicated above section (a) in black numbers and blue letters, respectively. This figure was generated using Ocean Data View (Schlitzer, R., Ocean Data View, odv.awi.de, 2017).



896

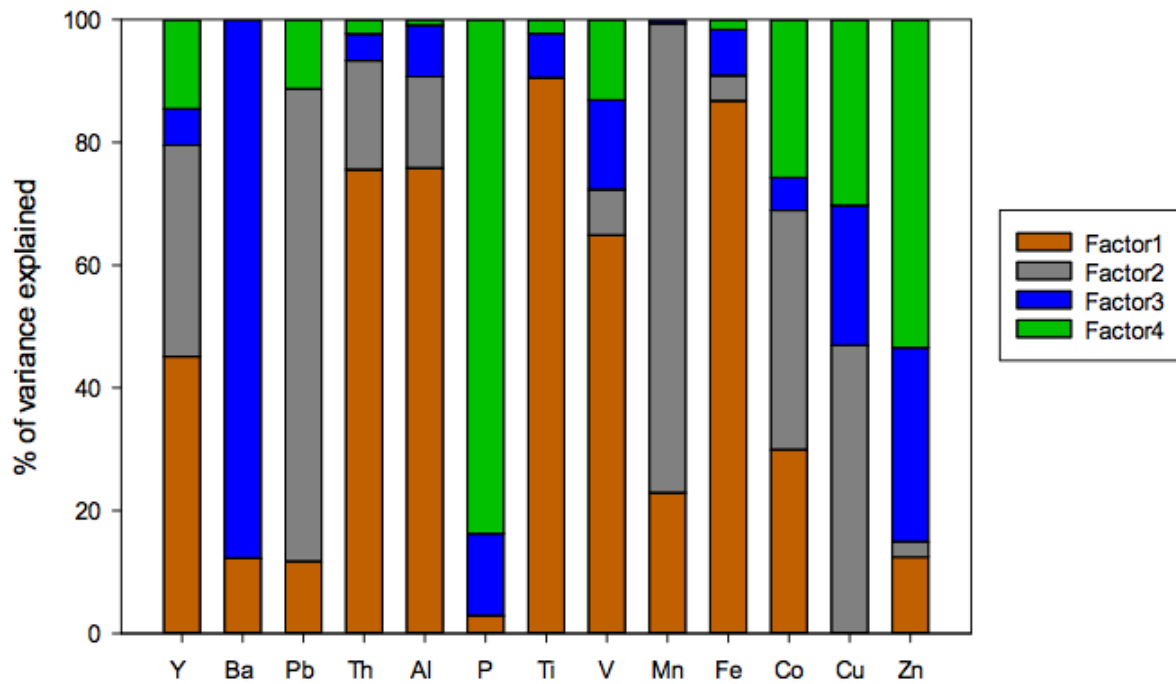
897

898

899

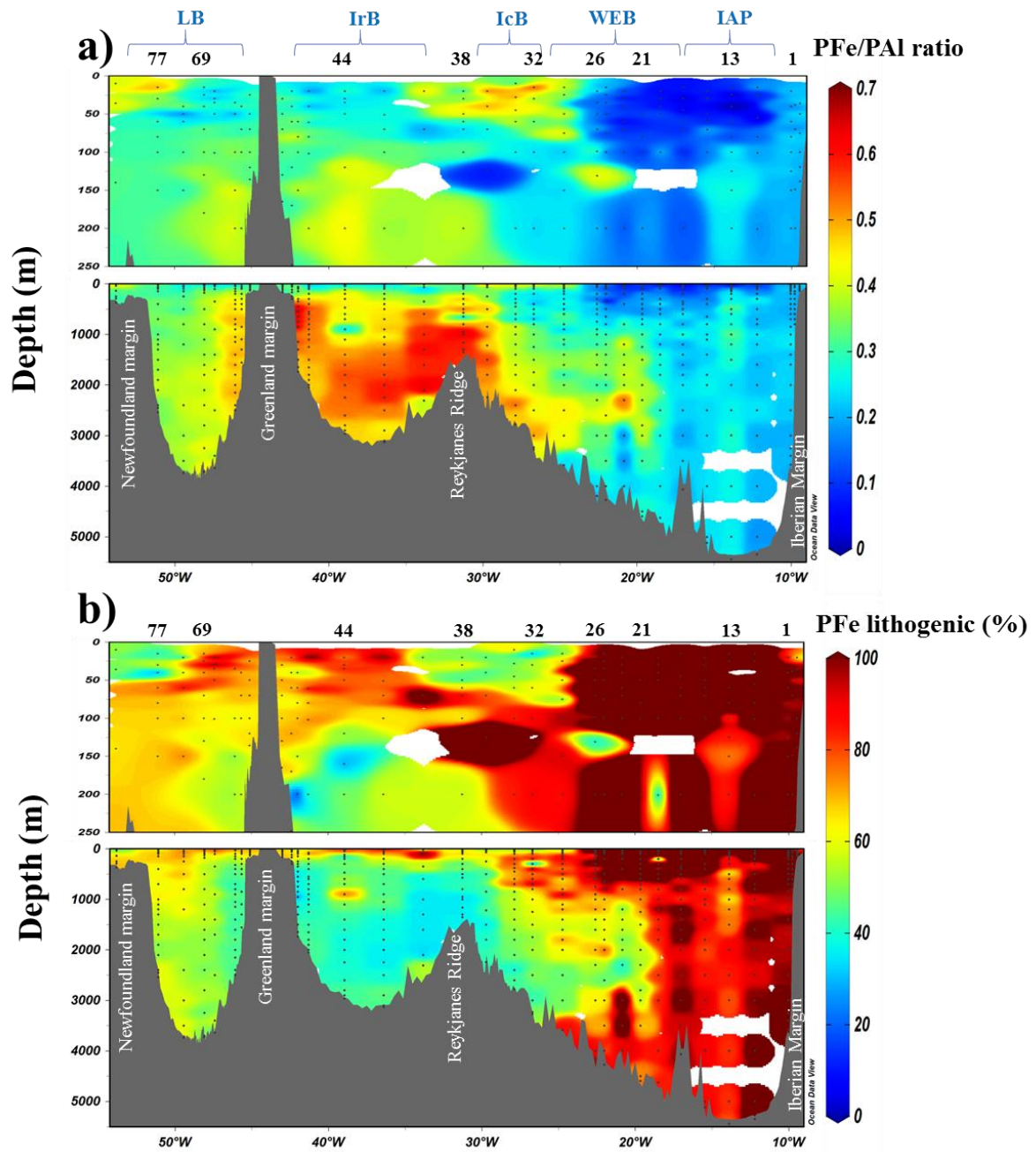
900

901 **Figure 5: Factor fingerprint of the positive matrix factorisation conducted on 445 particles samples collected along the**
 902 **GA01 section. The four main factors influencing the particulate trace element variance are represented in a stacked**
 903 **bar chart of the percentage of variance explained per element. Factor 1 is dominated by the lithogenic elements, e.g.**
 904 **Th, Al, Ti and Fe. Factor 2 is associated with Pb and Mn variances. Biogenic barite formation mainly influences factor**
 905 **3. Factor 4 is dominated by biogenic elements, e.g. P, Co, Cu and Zn.**



906
 907
 908
 909
 910
 911
 912
 913
 914
 915
 916
 917
 918
 919
 920
 921
 922
 923

924 **Figure 6: a) Section of the PFe to PAI molar ratio (mol mol⁻¹) during the GEOVIDE cruise (GA01) and (b) contribution**
 925 **(%) of lithogenic particulate iron (PFe_{litho}) based on Eq. (1). Station IDs and biogeochemical provinces are indicated**
 926 **above each section in black numbers and blue letters, respectively. This figure was generated using Ocean Data View**
 927 **(Schlitzer, R., Ocean Data View, odv.awi.de, 2017).**



928

929

930

931

932

933

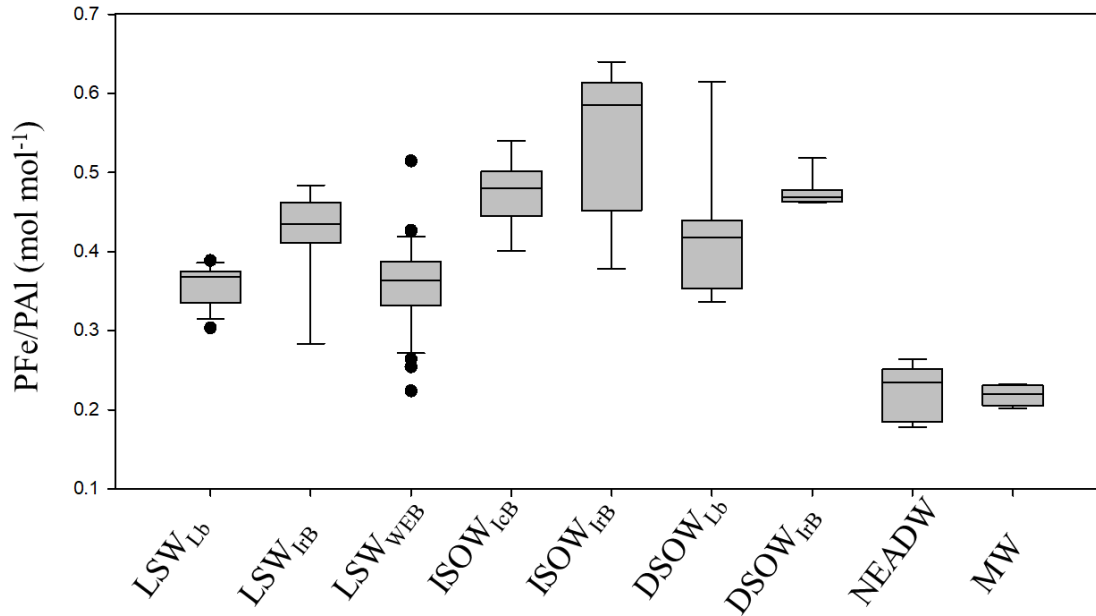
934

935

936 **Figure 7: Box and whisker diagram of PFe/PAI molar ratio in nine water masses sampled along the GA01 section in**
 937 **the North Atlantic Ocean. Water masses are defined in section 3.1 and in Figure 2. The PFe/PAI median values for each**
 938 **water masses with the biogeochemical provinces in subscript were as follows: $LSW_{LB} = 0.37$; $LSW_{IrB} = 0.44$; LSW_{WEB}**

939 = 0.36; ISOW_{ICB} = 0.48; ISOW_{IFB} = 0.58; DSOW_{LB} = 0.42; DSOW_{IFB} = 0.47; NEADW_{IAP} = 0.23; MW = 0.22 mol mol⁻¹.
 940 The difference in PFe/PAI between water masses is statistically significant (Kruskal-Wallis test; p = < 0.001 excluding
 941 water masses for which we had less than 5 data points for PFe/PAI). Noted that the UCC PFe/PAI ratio reported from
 942 Taylor and McLennan, (1995) is 0.21 mol mol⁻¹.

943



944

945

946

947

948

949

950

951

952

953

954

955

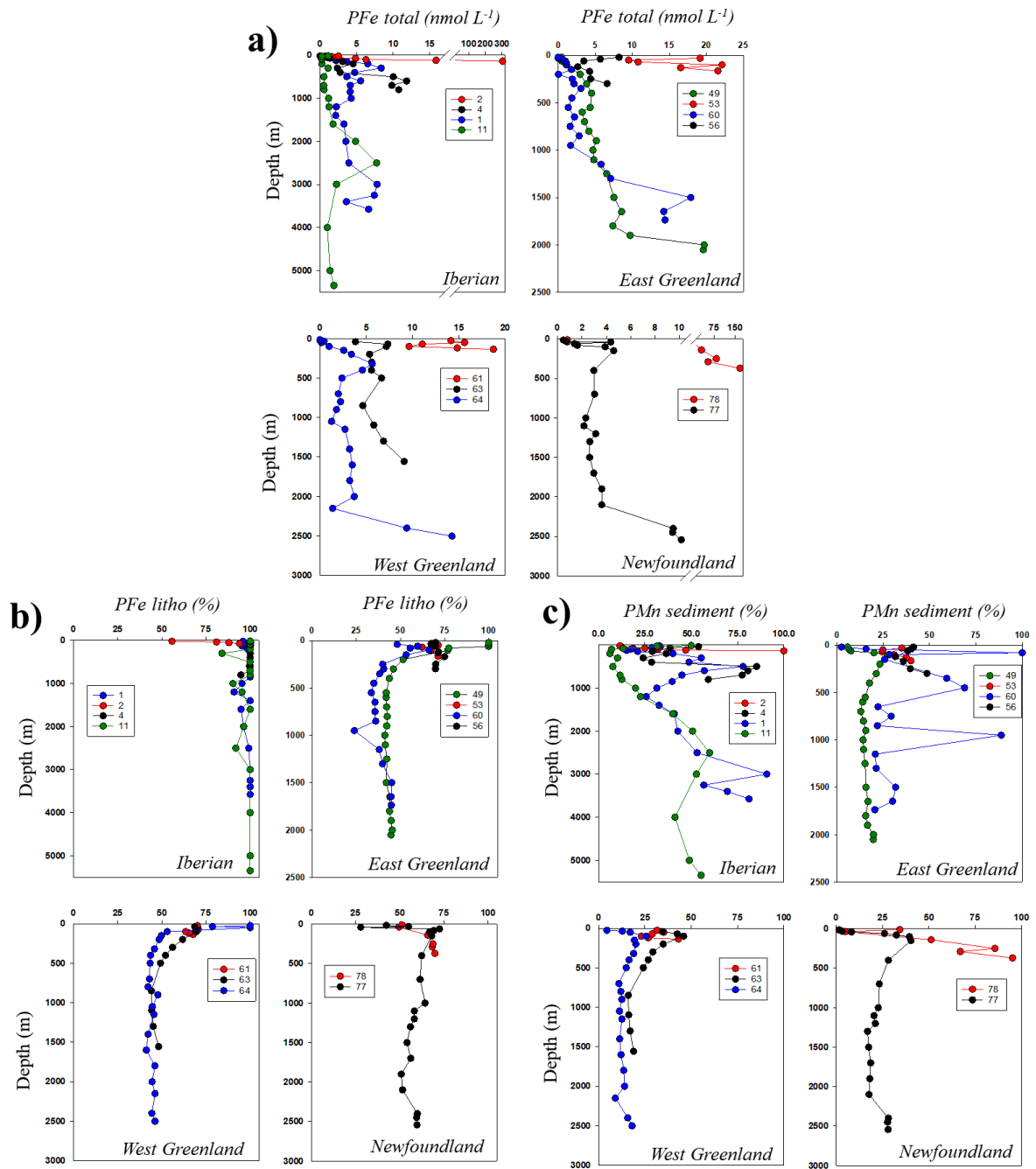
956

957

958

959

960 Figure 8: Vertical profiles of (a) PFe (nmol L⁻¹), (b) lithogenic proportion of particulate iron (PFe_{litho}, %) and (c)
 961 sedimentary proportion of particulate manganese (PMn sediment, %) at the Iberian, East-West Greenland and
 962 Newfoundland margins.



963

964

965

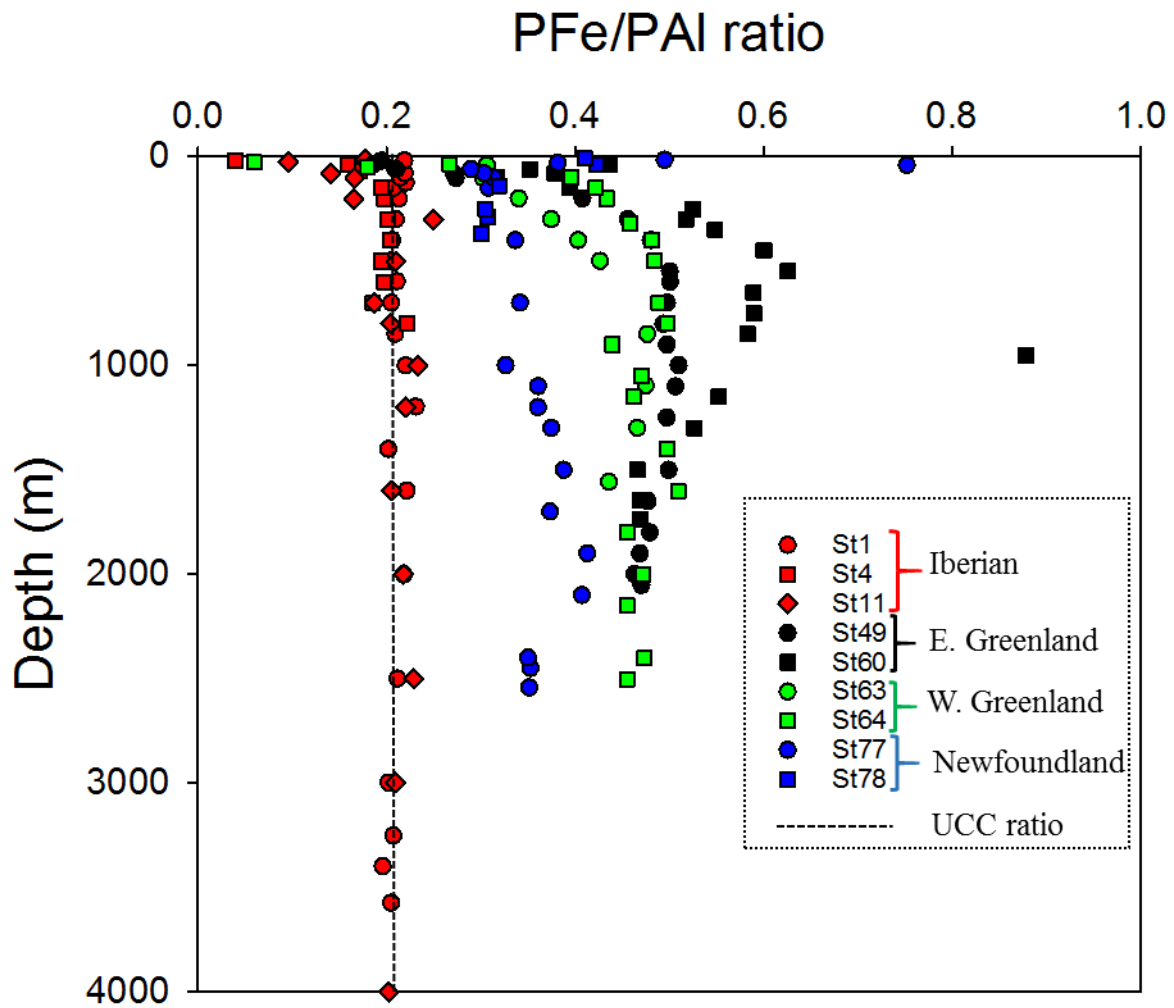
966

967

968

969

970 **Figure 9:** Scatter of the PFe/PAI ratio at the Iberian (red dots), East Greenland (black dots), West Greenland (green
 971 dots) and Newfoundland margins (blue dots). Dashed line indicate the UCC PFe/PAI ratio (Taylor and McLennan,
 972 1995).

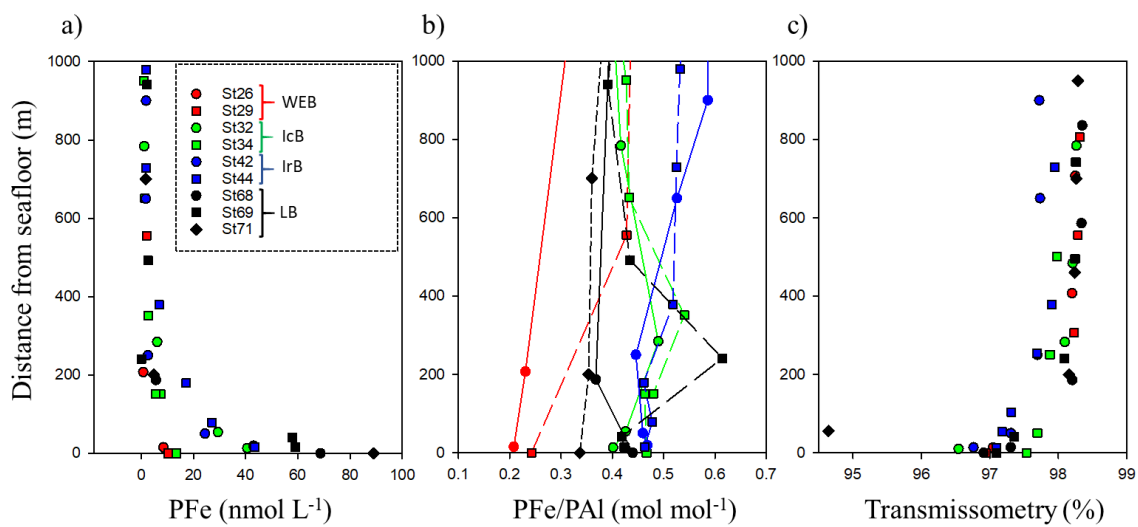


973
 974
 975
 976
 977
 978
 979
 980
 981
 982
 983

984 **Figure 10: Benthic Nepheloid Layers (BNLs) encountered along the GA01 section and observed through a) PFe total;**
 985 **b) PFe/PAI ratio and c) beam transmissometry (%) as a function of depth above the seafloor (m) at selected stations**
 986 **where a decrease in transmissometry was recorded in the West European (red dots), the Iceland (green dots), the**

987 **Irminger (blue dots) and the Labrador Basins. Noted that the UCC PFe/PAI ratio reported from Taylor and McLennan,**
988 **(1995) is 0.21 mol mol⁻¹.**

989



990

991

992

993

994

995

996

997

998

999

1000

1001

1002

1003

1004

1005

		Fe	Al	P	Mn
Blank (nmol L ⁻¹)	5µm filter	0.072	0.100	0.511	0.003
	0.45µm filter	0.132	0.164	1.454	0.005
Limit of detection (nmol L ⁻¹)	5µm filter	0.011	0.030	0.365	0.001
	0.45µm filter	0.026	0.046	1.190	0.001
Recovery CRM (%)	BCR-414 (n=10)	88 ± 7			94 ± 7
	MESS-4 (n=5)	98 ± 14	97 ± 14	80 ± 30	110 ± 18
	PACS-3 (n=8)	101 ± 9	99 ± 14	91 ± 34	112 ± 11

1006

1007 **Table 1: Blank and limit of detection (nmol L⁻¹) of the two filters and certified reference material (CRM)**
1008 **recoveries during GEOVIDE suspended particle digestions.**

1009

1010

Location	Depth range	PFe	PAI	PMn	PP	Fraction	Author	Year
N. Atlantic (>40°N)	All	bdl-304	bdl-1544	bdl-3.5	bdl-402	>0.45µm	This study	
Labrador Sea	0-250	0.1-1.2	0.1-1.5			>53 µm	Weinstein et al.	2004
Labrador Sea	0-250	2.5	3.6	0.05		0.4– 10µm	Weinstein et al.	2004
N. Atlantic (25-60°N)	Upper 1000m	0.29-1.71	0.2-19.7			0.4µm	Barrett et al.	2012
N. Atlantic	All	0-938	0-3600			0.8–51 µm	Ohnemus et al.	2015
Gulf of Maine	0-300	34.8	109			>0.4 µm	Weinstein et al.	2004
Eastern tropical N.A.	0-200		0.59-17.7			>0.2 µm	Dammshausen et al.	2013
Eastern tropical N.A.	0-600	ND-12				1–51 µm	Lam et al.	2012
Sub-tropical N.A.	All	ND-140	ND-800			>0.45µm	Milne et al.	2017
Meridional Atlantic	0-200		0.35-16.1			>0.2 µm	Dammshausen et al.	2013
Northeast Pacific	0-3557		0.0-54.2			1-53µm	Sherrell et al.	1998
Eastern tropical S.Pacific	All	bdl-159	bdl-162	bdl-8.7	bdl-983	>0.8 µm	Lee et al.	2017
South Georgia Shelf	All	0.87-267	0.6-195	0.01-3.85		>1 µm	Schlosser et al.	2017
Southern Ocean	30-340	0.15–13.2	0.11–25.5			>53 µm	Planquette et al.	2009
East Antarctic	Surface		0.02-10.67	0.01-0.14		>0.2 µm	Lannuzel et al.	2011
East Antarctic	Fast ice	43-10385	121-31372	1-307		>0.2 µm	Lannuzel et al.	2014
Ross Sea	All	0.68-57.3	ND-185	ND-1.4	5.4-404	>0.4 µm	Marsay et al.	2017

1011

1012 **Table 2: Concentration (in nmol L⁻¹) of particulate trace elements (PFe, PAI, PMn and PP) in suspended**
1013 **particles collected in diverse regions of the world's ocean. Bdl: below detection limit, ND: non-determined.**

1014

1015